Article DOI: 10.1144/SP484-2018-43

Article number: GSLSpecPub18-043

To cite this article, please follow the guidance at https://www.geolsoc.org.uk/onlinefirst#citations

Instructions

1. **We need to clearly see the changes you have made.**
   Do: annotate PDF using the comment facility, or provide a separate list of your corrections using line numbers.
   Don't: send a revised word file of your manuscript or internally edit the PDF. Help on making proof corrections is available at http://www.geolsoc.org.uk/ProofCorrections
2. **Proofs (typeset version) should not be posted to any website or server.** You can post the accepted (pre-typeset) manuscript 12 months after online publication or the original (i.e. not peer reviewed) manuscript now. These proofs are for checking purposes only. They should not be considered as final publication format and must not be used for any other purpose. Please do not print and distribute multiple copies. Neither excerpts nor the article in its entirety should be included in other publications until the final version has been published and citation details are available. Please see our Terms and Conditions at https://www.geolsoc.org.uk/Publications/Lyell-Collection/Using-the-Lyell-Collection/Copyright-Permissions-and-Terms-of-Use/Copyright-Policy-and-Terms-of-Use-for-Authors
3. **Permissions:** Permission to reproduce any third-party material in your paper should have been obtained prior to acceptance. If your paper contains figures, tables or text requiring permission to reproduce, and you have not already obtained that permission, please inform me immediately by email.
4. **Check this proof carefully for errors:** Once it is published online no further changes can be made.
5. **References:** All references to papers in this volume will be dealt with by the production editor.
6. **Figures and tables:** Please check that they are complete and the correct content and legend are present. Figures in the proof are low-resolution versions that will be replaced with higher resolution versions when the paper is published.
7. **Special characters:** Please check that special characters, equations, taxonomy and units, if applicable, have been reproduced accurately.
8. **ORCID IDs:** Only those supplied at submission stage appear on this proof. Additional ORCID IDs can be added as part of your corrections.

Funding information

- Only funding information supplied at submission (shown in the table below) will be transmitted to CrossRef, assuming the mandatory fields are complete. Please provide additional information in the table below if required.
- Instructions on how to add missing or additional funding information can be found at http://www.geolsoc.org.uk/ProofCorrections
- Please note that providing additional funding information does not alter the text in the Funding section of your proof. If you have any changes to this section, please provide as part of your corrections.

Funding agency (mandatory)	Funding agency ID (mandatory)	Grant number (optional)	Principal award recipient
	Author to provide ID		

Please answer all queries

No	Query
Q1	Please check this proof carefully for errors, once it is published online no further changes can be made. In particular, check author names, affiliations & corresponding email address and that figures, tables and equations are correct. Also, please check your proof to ensure you have acknowledged your funding source (if applicable).
Q2	Please give PVT in full.
Q3	There is no part (d) inside figure 13. Please provide if needed.

A renewed look at calcite cement in marine-deltaic sandstones: the Brent Reservoir, Heather Field, Q1 northern North Sea, UK

RICHARD H. WORDEN[1]*, GLENN T. MORRALL[1], SEAN KELLY[2], PETER Mc ARDLE[2] & V. BARSHEP[1]

[1]*School of Environmental Sciences, University of Liverpool, Jane Herdman Building, 4 Brownlow Street, Liverpool, UK, L69 3GP*

[2]*EnQuest plc, Annan House, Palmerston Road, Aberdeen, AB11 5QP, UK*

R.H.W., 0000-0002-4686-9428

**Correspondence: r.worden@liv.ac.uk*

Abstract: Wireline and seismic acoustic impedance imaging show that the marine part of the clastic Brent Group reservoir in the Heather Field, northern North Sea, contains much calcite cement in the flank parts of the structure. The non-marine Ness Formation and crest parts of the structure contain negligible calcite cement. This localized calcite cement has led to relatively poor reservoir performance since first oil in 1978, although a new suite of wells has boosted production with plans to keep the field active until 2030. Understanding the origin and distribution of calcite cement would help the development of more realistic reservoir models and boost production rates through optimum well location. We have thus used a suite of techniques, including standard point counting, SEM-EDS mineralogy, BSE microscopy, fluid inclusion thermometry and stable isotope analysis, to develop new and improved models of calcite distribution. Calcite seems to have attributes of both early and late diagenetic cement. A 30–40% intergranular volume in calcite cemented beds seems to support pre-compactional growth but high-temperature fluid inclusions and the presence of primary oil inclusions suggest late growth. Much calcite may have developed early but it seems to have recrystallized, and possibly undergone redistribution, at close to maximum burial or had a late growth event. Calcite cement probably originated as marine-derived micrite, bioclasts or early marine cement but adopted the isotopic characteristics of high-temperature growth as it recrystallized. Quartz grains have corroded outlines in calcite-cemented areas with one sample, with 79% calcite cement, displaying signs of nearly total replacement of quartz grains by calcite. The flank localization of calcite remains to be explained, although it could be due to primary depositional factors, early diagenetic loss of calcite from crestal regions or late diagenetic loss of calcite from crestal regions. Controversially, the growth of calcite seems to be associated with quartz dissolution, although the geochemical and petrophysical cause of this remains obscure. Diagenetic loss of quartz from sandstones cannot easily be explained by conventional modelling approaches and yet seems to be an important phenomenon in Heather sandstones.

Background to the question of porosity-destroying calcite in the Heather Field

Understanding the origin of pervasive calcite cement in sandstone reservoirs can be critical to the successful development of a model of calcite distribution. Such a model could be used in planning production optimization by informing well placement and completion strategies. The Middle Jurassic Brent Group reservoir in the Heather oil field locally has large quantities of calcite cement (Glasmann *et al.* 1989*b*) that have contributed to the complexity of the reservoir and led to slower oil production and a lower recovery than was planned at the start of field life in the 1970s.

Owing to extensive exploration, appraisal and development drilling in the Brent Province, a substantial literature on the diagenesis of the Brent Group reservoirs has developed (Bjørlykke *et al.* 1992; Giles *et al.* 1992; Prosser *et al.* 1993; Lundegard 1994; McAulay *et al.* 1994). Despite the maturity of the oil fields in the northern North Sea, the area is still of significant interest owing to ongoing production from many fields, such as Heather and Thistle, and ongoing interest in the development of satellite structures. Understanding diagenetic changes is important because the combination of compaction, cement growth, mineral dissolution and mineral replacement typically has a substantial influence on porosity and permeability and thus field development (Worden *et al.* 2018*a*). Study of the Brent Group has revealed a diverse suite of

From: Dowey, P., Osborne, M. & Volk, H. (eds) *Application of Analytical Techniques to Petroleum Systems*. Geological Society, London, Special Publications, **484**,
https://doi.org/10.1144/SP484-2018-43

diagenetic dissolution and precipitation processes, including eogenetic calcite, siderite and quartz growth, followed by feldspar dissolution, kaolinite growth, further carbonate cementation and late precipitation of quartz cement and authigenic illite (Bjørlykke *et al.* 1992). Reconstructing the relative timing of diagenetic events in Brent reservoirs has been controversial owing to inconsistencies in the interpretation of textural relationships between diagenetic minerals and overprinting of early diagenetic processes by burial diagenetic processes (Bjørlykke *et al.* 1992). Continued sedimentary, petrographic, geochemical and petrophysical analyses and research into the diagenesis of the Brent Group reservoirs has led to conflicting interpretations of various diagenetic mineral dissolution and precipitation events, and the subsequent creation of diagenetic models (Harris 1989, 1992; Bjørlykke *et al.* 1992; Giles *et al.* 1992; Glasmann 1992; Haszeldine *et al.* 1992; Nedkvitne & Bjørlykke 1992; Hogg *et al.* 1993; Lundegard 1994; McAulay *et al.* 1994; Morad & De Ros 1994; Osborne *et al.* 1994; Prosser *et al.* 1994, 1993; Benbaccar *et al.* 1995; Hogg *et al.* 1995; Ashcroft & Ridgway 1996; Ehrenberg 1997; Potdevin & Hassouta 1997; Guilhaumou *et al.* 1998; Hassouta *et al.* 1999; Walderhaug 2000; Ehrenberg & Jakobsen 2001; Girard *et al.* 2001; Ziegler *et al.* 2001; Girard *et al.* 2002; Brosse *et al.* 2003; Sanjuan *et al.* 2003; Munz *et al.* 2004; Wilkinson *et al.* 2004; Clauer & Liewig 2013).

The Heather Field

The Heather Field is in Block 2/5 of the UK sector of the northern North Sea, at the western margin of the East Shetland basin, 90 miles (144 km) NE of the Shetland Isles (Fig. 1). The Field was discovered in 1973 and production began in 1978.

Before production commenced, the Heather Field was estimated to contain 438 MMBBL in place, 100 MMBBL of which was originally estimated to be recoverable (Penny 1991). Production from the Brent Group reservoirs of the Heather Field started in 1978 and peaked at 38 000 BOPD in 1982, after which there was a steady decline in production to the present value of around 6000 BOPD. In 2003, it was reported that the field had an original in-place of 464 MMSTB and had produced 120 MMSTB

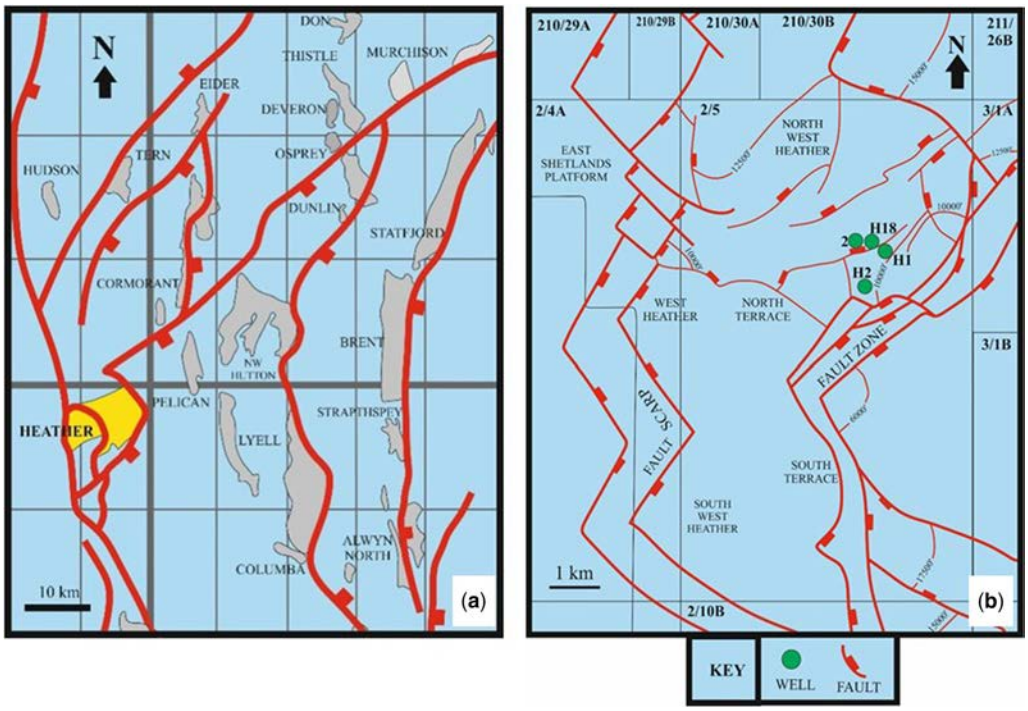

Fig. 1. (**a**) Location map of the UK sector of the northern North Sea. The Heather Field is highlighted in yellow. Major faults show the structural relationship to other Brent Group oil fields; adapted after Kay & Cuddy (2002). (**b**) Location map of the Heather Field. Note the locations of the four wells sampled (2/5-H1; 2/5-H2; 2/5-2; 2/5-H18). The top of the Brent structure is marked by structure contours. Major faults are also highlighted; adapted from Glasmann *et al.* (1989*a*).

during 25 years of activity (Kay 2003). Recent re-evaluation of the reservoir led to an estimate that there was still 360 MMBBL oil in-place (EnQuest 2018) after *c.* 40 years of production. The current operator, EnQuest, has undertaken a redevelopment programme that aims to extend the life of the Heather Field until 2030 (EnQuest 2018).

The Middle Jurassic Brent Group consists of five lithostratigraphic units (Fig. 3): the Broom, Rannoch, Etive, Ness and Tarbert Formations (Deegan & Scull 1977). The first four units (Broom to Ness) represent a broadly progradational succession. The Broom Formation is characterized by medium- to coarse-grained, poorly sorted, locally carbonate-cemented sandstones, deposited as delta front splays (Richards 1992; Hampson *et al.* 2004). The Rannoch Formation comprises fine-grained, micaceous sandstones that record reworking of progradational, wave-dominated, delta sediments to lower-middle shoreface sediments influenced by wave and basinal processes (Richards 1992; Morad & De Ros 1994; Prosser *et al.* 1994; Loseth & Ryseth 2003; Helle & Helland-Hansen 2009). Persistent progradation of the wave-dominated delta led to the deposition of fine- to medium-grained, massive upper-shoreface sandstones of the Etive Formation (Loseth & Ryseth 2003; Helle & Helland-Hansen 2009), and the delta plain deposits of the Ness Formation (Ryseth 2000; Went *et al.* 2013). The overlying Tarbert Formation comprises coarse- to very-coarse-grained, micaceous and bioturbated sandstones that record a transgressive lag over the top of the delta during a rise in relative *sea-level* (Ronning & Steel 1987; Richards 1992; Hampson *et al.* 2004). The source rock for the oil, typical of the North Sea, was the Upper Jurassic Kimmeridge Clay Formation; maturation of the source rock and filling of the Heather reservoir was originally interpreted to be relatively late, from about 20 to 25 Ma (Glasmann *et al.* 1989*b*).

Oil is produced from the deltaic and shallow marine Middle Jurassic Brent Group in the Heather Field at depths of between 9500 and 11 600 ft. (2895–3536 m) TVDss. The main Heather Field structural trap comprises a mid-Jurassic, NW-tilted fault block, 7 miles (11.2 km) long from NW to SE and 5 miles (8 km) wide from NE to SW (Penny 1991). The trap, like those in other mid-Jurassic traps of the northern North Sea, initially formed as a result of extension-related faulting in the Jurassic (reflected in the burial curve illustrated in Fig. 2). Rotation of tilted fault blocks, soon after the end of the deposition of Brent Group sediment, led to erosion of part of the reservoir over the crest of the Heather Field. The Broom Field, produced via a subsea tieback to the Heather Platform, lies directly to the west of the Heather Field and is bounded to the west by the East Shetland Platform Boundary Fault. Intense faulting has divided the Heather

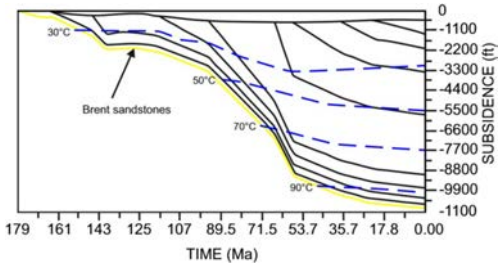

Fig. 2. Burial history of the Brent sandstones (yellow) in a typical Heather Field well, illustrating the subsidence and temperature history (dashed blue lines); adapted after Glasmann *et al.* (1989*a*).

Field reservoir into nine discrete fault blocks (Fig. 1) which have limited or no inter-block communication. Shales and siltstones of the Heather Formation cover the trap at all elevations and provide the top-seal for the reservoir (Glasmann *et al.* 1989*b*).

Some parts of the Heather Field have good inter-well connectivity between injectors and producers but there are other parts that have poor inter-well connectivity. There are extensive zones and areas of unswept oil within parts of the Heather Field that are now assumed to be a consequence of reduced reservoir quality and compartmentalization owing to localized calcite cementation. The complexity of the reservoir in terms of diagenetic compartmentalization was not suspected at the start of field-life. The ability to predict the areal distribution of calcite-cemented horizons would provide a valuable tool which would help bypassed oil to be accessed. By analogy, this diagenetic model could aid in the development of less mature oil provinces. In order to understand the distribution of calcite cementation it is important to understand the origin and timing of calcite cementation and their relationship to oil emplacement within the Brent Group.

Initial interpretation of calcite in the Broom Formation, Heather Field

Previous studies of the Heather Field concluded that calcite cementation occurred at burial depths of less than about 670 m (and thus temperatures of less than about 40–50°C) (Glasmann *et al.* 1989*a*, b). This interpretation was based on locally elevated intergranular volumes (up to 40%) including the complete occlusion of porosity in some layers, the interpretation of continued early diagenetic processes such as K-feldspar dissolution and kaolinite growth following calcite growth, calcite cement within tectonically early fractures (Glasmann *et al.* 1989*b*).

The abundant calcite cement found in the Heather Field was interpreted to be the result of meteoric water influx (Glasmann *et al.* 1989*b*). This meteoric-

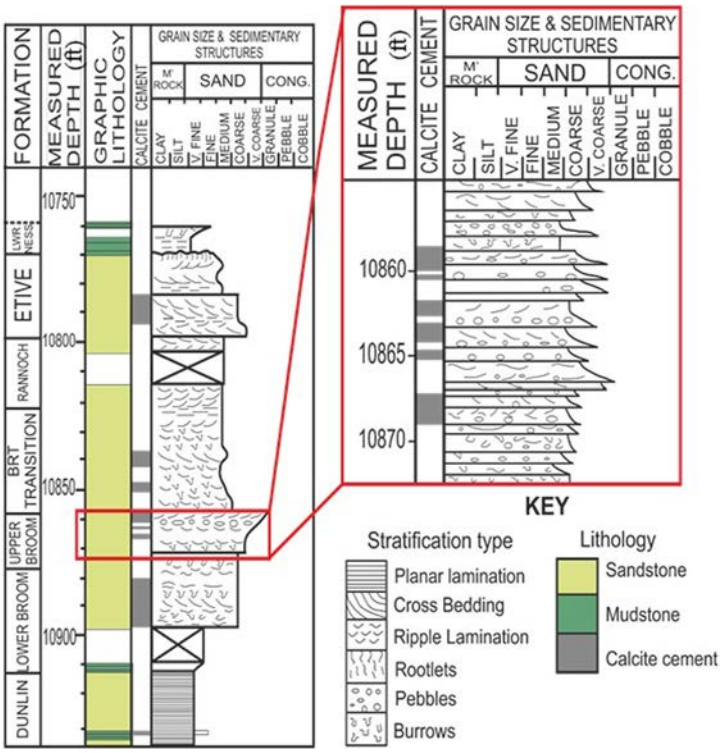

Fig. 3. Schematic sedimentary log of the core from well 2/5-2. Sedimentary facies are marked up until the lower portion of the Lower Ness (no core available at a shallower depth than that marked by the dashed line). Calcite cement is more abundant in the lower part of the Brent compared with the upper part of the Brent. The blue box shows a portion of the schematic sedimentary log in more detail.

derived water was interpreted to have contained variable amounts of reduced Fe and Mn based on cathodoluminescence patterns in fracture-filling calcite cement (i.e. the water was no longer in communication with the atmosphere). Calcite cement was shown to have radiogenic Sr isotope values higher than those of coeval marine-derived calcite, but the calcite cement was also reported to have lower Sr concentrations than is typical of marine calcite. The oxygen stable isotope values for the calcite cement were also shown to be variable from about −8 to about −15‰ VPDB with a mean of −11.2‰ VPDB. The interpreted growth temperature of 40–50°C was used to infer that the water that caused calcite cementation had a $\delta^{18}O$ value of about −4 to −6‰ VSMOW, which seemed to support the meteoric origin of the calcite cement.

The carbon stable isotope values for the calcite cement were shown to be variable, ranging from about −4 to about −28‰ VPDB, with the low values interpreted to signify input of organic-derived CO_2 and the higher values inferred to be derived from atmospheric sources (i.e. meteoric water). Glasmann *et al.* (1989*b*) reported that shell fragments were extremely rare and that there seemed to be a lack of calcite at the crest of the field, in areas associated with the end-of-Brent erosion event. They also reported a local association with faults. Overall, Glasmann *et al.* (1989*b*) concluded that calcite cement was an early diagenetic phenomenon that resulted from meteoric influx during end-of-Brent erosion, long before deposition of the Kimmeridge Clay Formation, and necessarily at relatively shallow depth and low temperature.

In this study we present new data on the growth temperatures of calcite, based on aqueous fluid inclusion homogenization temperatures. We also present new petrographic data, including UV and SEM-EDS images, to reinterpret the timing of calcite growth. We also examine data from other studies of pervasive calcite cementation in sandstones including several studies of other Brent Group reservoirs. We will re-examine the depositional context of the pervasive calcite cementation in the Heather Field and reconsider the significance of the C, O and Sr isotope data.

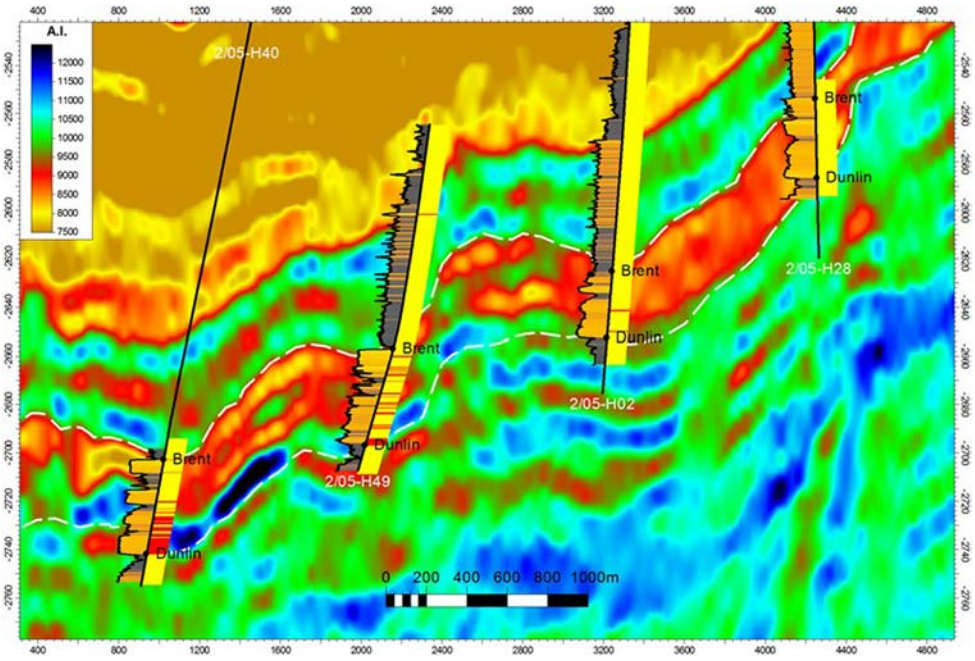

Fig. 4. Seismic data from the Heather Field represented in terms of acoustic impedance with gamma ray logs from four wells added for reference. White dashed lines represent the approximate top and base Brent horizons. To the right of the gamma ray log is a calcite flag, determined from sonic and density logs, marked as a red bar. Yellow/red indicates low impedance; dark blue/green indicates high impedance. Low impedance thus represents low-calcite cement and high-porosity zones and high impedance represents high-calcite cement and low-porosity zones. Crestal areas of the field are largely free of calcite cement, whereas downdip areas are locally heavily cemented. Calcite-cemented horizons appear to be strata-bound to some extent and locally follow certain intervals which may be correlative. Note that there is no simple relationship between present-day structural depth and calcite abundance.

Oil field data

Seismic data, converted to acoustic impedance using standard industry techniques, have been provided by EnQuest (Fig. 4). Neither seismic data nor well-log data are the main focus for this study, but they are used to frame the research questions posed. The seismic acoustic impedance data suggest that crestal areas of the field generally have low impedance, typical of high-porosity sandstones (Fig. 4). In contrast the downdip areas can have higher impedance values, typical of low-porosity sandstones (Fig. 4). The downdip areas have variable impedance with the stratigraphically lower and structurally deeper part of the Brent tending to have the highest impedance values with the stratigraphically upper and crestal parts of the Brent successions retaining the low impedance (Fig. 4). Since high impedance is typical of tight rock (i.e. with low porosity), the primary assumption to take from the seismic impedance data is that downdip parts of the lower part of the Brent succession are tightly cemented.

Wireline and core analysis data for wells 2/5-2, 2/5-H01, 2/5-H02 and 2/5-H18 were provided by EnQuest. Where calcite-cemented zones exhibit 30–40% calcite by volume, there is a significant impact on log responses. The wireline logs here reveal calcite-cemented horizons based on reduced transit time, increased bulk density and high resistivity values (Figs 5 & 6). This is expressed in the lower cumulative thickness of calcite-cemented horizons in the crestal wells (e.g. 15 ft. (4.6 m) in 2/5-H1; Fig. 5) compared with the structurally deeper wells (e.g. 67 ft. (20.4 m) in 2/5-H18; Fig. 6). The wireline log response suggests that the thickest continuously calcite-cemented interval is *c.* 15 ft. (4.6 m) in well 2/5-H18; Fig. 6). As seen in core and wireline logs, it appears that the Broom Formation exhibits the highest calcite cement abundance and the Ness Formation has the lowest abundance.

Materials and methods

Nineteen samples were collected from cores of variably calcite-cemented sandstones from wells 2/5-2, 2/5-H01, 2/5-H02, 2/5-H18. The facies, depositional environment and carbonate-cemented intervals in

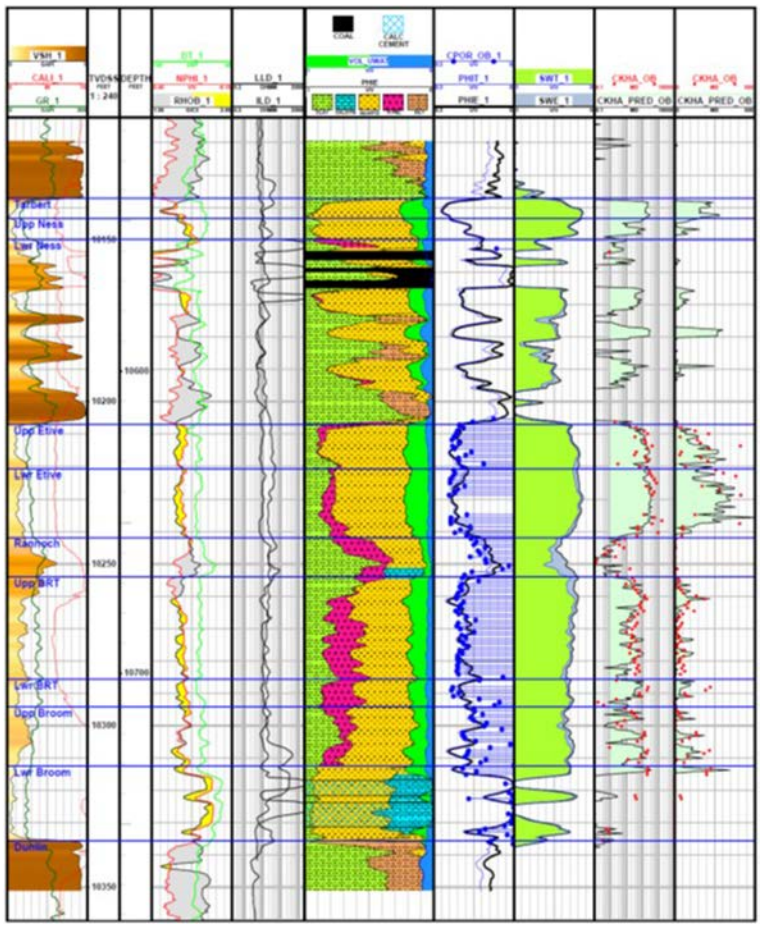

Fig. 5. Interpretation of the wireline log suite from well 2/5-H1, which is considerably updip of well 2/5-H18 (Fig. 6). CALI, calliper log; GR, gamma ray log; VSH, VShale; DT, sonic log; NPHI, neutron log; RHOB, density log; LLD and ILD, deep resistivity logs; PHIE, log-derived porosity; CPOR, core analysis porosity; PHIT, total porosity; PHIE, effective porosity; SW, water saturation; CKHA, core analysis permeability. Note that the formation tops have been picked for the Dunlin Group, Lower Broom, Upper Broom, Lower Broom–Rannoch Transition (Lwr BRT), Upper Broom Rannoch Transition (Upp BRT); Rannoch, Lower Etive, Upper Etive, Lower Ness, Upper Ness and Tarbert. Calcite-cemented horizons are identified based on their reduced transit time (around 60 μs/ft; DT), increase in density, porosity values close to 0 p.u. and high-resistivity spikes. The cumulative thickness of the calcite-cemented horizons is 15 ft.

each core were interpreted. Samples were obtained from a variety of lithologies in order to represent the variability in the sedimentology throughout the Brent succession.

SEM, CL and optical microscopy

Stained thin sections and polished thin sections were prepared from all 19 core samples. Sections were cut perpendicular to bedding to reveal depositional and diagenetic features. All polished sections were impregnated with blue-dyed araldite resin to ensure the easy identification of pore space. Thin sections were stained for carbonates and feldspars. Light microscopy was undertaken using an Olympus BX51 microscope. Backscattered scanning electron microscopy (BSEM) was carried out using a Hitachi TM3000 table-top SEM at an accelerating voltage of 5 or 15 kV and a working distance of 17.5 mm. The relative timing of growth of calcite was ascertained by determining whether a mineral had overgrown crystal faces of an earlier growing mineral.

Sandstone modal composition was obtained in the laboratories at the University of Liverpool by

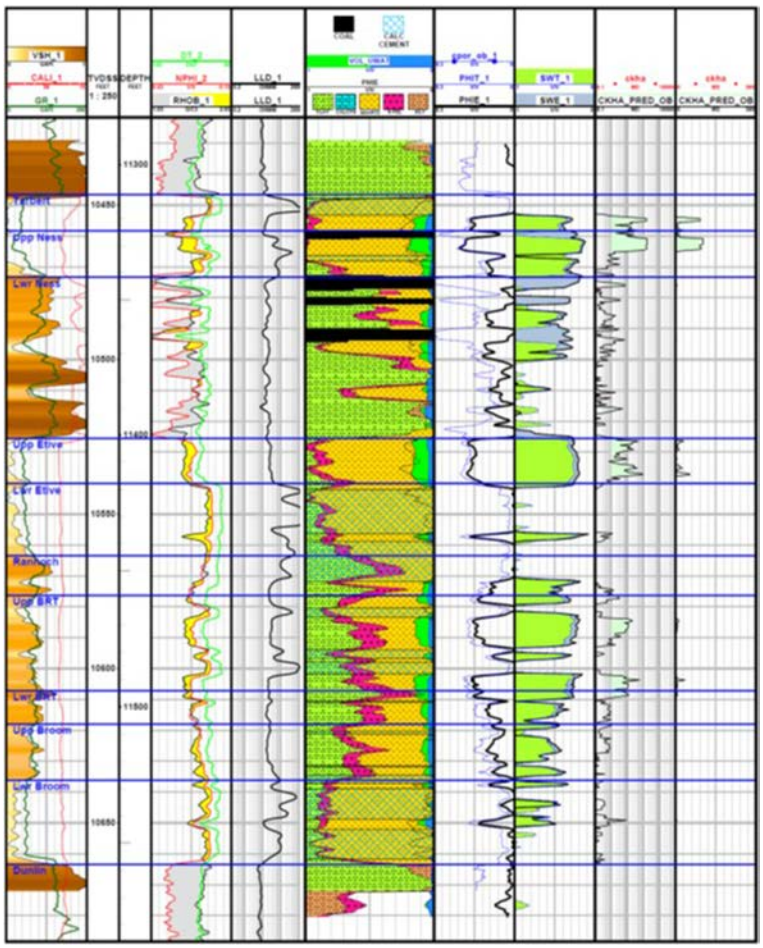

Fig. 6. Interpretation of the wireline the wireline log suite from well 2/5-H18, which is considerably downdip of well 2/5-H1 (Fig. 5). CALI, calliper log; GR, gamma ray log; VSH, VShale; DT, sonic log; NPHI, neutron log; RHOB, density log; LLD and ILD, deep resistivity logs; PHIE, log derived porosity; CPOR, core analysis porosity; PHIT, total porosity; PHIE, effective porosity; SW, water saturation; CKHA, core analysis permeability. Note that the formation tops have been picked for the Dunlin Group, Lower Broom, Upper Broom, Lower Broom–Rannoch Transition (Lwr BRT), Upper Broom Rannoch Transition (Upp BRT); Rannoch, Lower Etive, Upper Etive, Lower Ness, Upper Ness and Tarbert. Calcite-cemented horizons are identified based on their reduced transit time (around 60 μs/ft; DT), increase in density, porosity values close to 0 p.u. and high resistivity spikes. The cumulative thickness of the calcite-cemented horizons is *c.* 67 ft.

point counting all 19 thin sections at 300 counts per section. Point counting was performed using a Petrog stage (Conwy Valley System Ltd (CVS), UK) on an Olympus BX51 microscope with a ×10 objective, but higher-power objectives were used where necessary, e.g. for finer grained materials and grain coatings. Textural analysis was performed on 200 grains per sample using the Petrog system. The grid-spacing for point counting was selected to ensure that the whole thin section was covered. Quartz cement was differentiated from quartz grains by observing the presence of a trail of inclusions on quartz grain surfaces and by the presence of a euhedral outline to the quartz cement.

SEM-EDS analysis

Quantitative evaluation of minerals by scanning electron microscopy (QEMSCAN®, but generally referred to as SEM-EDS) was used to give spatially resolved mineralogy for the 19 selected samples based on elemental chemistries using polished thin sections (Pirrie *et al.* 2004; Armitage *et al.* 2010; Worden *et al.* 2018*b*). QEMSCAN® is the

proprietary name for rapid, repeatable automated mineralogical SEM-EDS analysis developed by FEI. The outputs are detailed and repeatable mineral quantification and maps of mineral distribution that reveal the fabric of the rock. The SEM-EDS was equipped with two high-speed EDS detectors configured to acquire chemical data from secondary X-rays by single or dual EDS detectors, at spatially pre-defined points, across any polished solid sample. The distance between these points on any given grid is user-defined depending primarily on what the data are to be used for. Owing to the physics of electron beam–sample interaction, there is a minimum practical spacing (resolution) of just less than 1 μm. However, wider step sizes between the points are possible, resulting in a pixellated image with lower than optimum spatial resolution. Once the elemental concentration has been measured at each point by the EDS detectors, the software automatically matches the EDS spectrum to a library of mineral definitions. These mineral definitions are called SIPs (species identification protocols) and are assembled in an SIP list that is effectively an archived mineral library. Each mineral is assigned a colour, and these data points are combined to form a contiguous false colour image of the sample. In addition to the images, the sum of each occurrence of an identified mineral is tabulated so that minerals and groups of minerals may be quantified.

Fluid inclusion analysis

Six doubly polished fluid inclusion wafers (100 μm thick) were prepared from highly calcite-cemented samples. Each wafer was impregnated at room temperature with blue-dyed epoxy resin. Fluid inclusion petrography of the calcite cement was undertaken using an Olympus BX51 petrographic microscope fitted with high-powered objectives. A Linkham THMSG600 thermometric stage was used to measure homogenization temperatures (*Th*) during microthermometric analysis. A peripheral UV light generator was used to assess for the presence of oil inclusions, since hydrocarbons fluoresce when subject to a UV light source. An Olympus DP71 digital camera captured images of aqueous and oil inclusions. Room-temperature calibration of the thermometric stage was done using a synthetic fluid inclusion. Homogenization temperatures were taken for 93 two-phase aqueous fluid inclusions from the fluid inclusion wafers. Fluid inclusions were difficult to identify in some parts of the sections owing to clouding by clay minerals (in particular kaolinite) that were locally intergrown with calcite. The *Th* techniques adopted for primary inclusion in calcite followed best practice described by Goldstein & Reynolds (1994).

Stable isotope analysis

SEM-EDS and XRD analyses revealed that 16 out of the 19 analysed samples contained enough calcite for stable isotope ($\delta^{13}C$ and $\delta^{18}O$) analysis. Stable isotope analyses were carried out on these 16 samples at the University of Liverpool isotope laboratory. CO_2 was extracted by dissolving the crushed sample in 10% phosphoric acid. The evolved CO_2 gas was analysed in a SIRA10 mass spectrometer (24 h). $\delta^{13}C$ and $\delta^{18}O$ values are presented as parts per mil (‰) relative to the standard Vienna-Peedee Formation Belemnite (VPDB). Results are analytically correct within 0.1‰ VPDB and 0.2‰ VPDB for carbon and oxygen respectively.

Results

Core description

Calcite cement exhibits a range of growth forms in core, including centimetre-scale discrete nodules (Fig. 7b) to coalesced nodules and fully cemented strata-bound horizons (Fig. 7a). Nodule and cemented horizons range from white/light grey to cream/pale yellow. Calcite growth around stylolites (representing mesogenetic compaction) is visible in core (Fig. 7b). Zones of pervasive calcite cementation occur in a variety of facies associations (Fig. 3). Calcite cement occurs in the marine portions of the Brent of the Heather Field, including the Broom, Rannoch, Etive and Tarbert (Bjørlykke *et al.* 1992). The most abundant calcite cement occurs in the Broom Formation. The non-marine Ness Formation is relatively free of calcite (Figs 5 & 6).

Petrographic data

The Broom Formation sandstones are variably calcite cemented, sub-arkosic and micaceous arenites. Detrital grains include the dominant mono- and polycrystalline quartz and K-feldspar, and minor muscovite, illitic-matrix, rutile and a variety of heavy minerals (Table 1). The main diagenetic mineral found in these Broom samples is calcite with minor K-feldspar and quartz overgrowths and minor pore-filling kaolinite, illite and pyrite (Table 1). The calcite-cemented samples have low porosity with primary intergranular porosity being dominant.

Samples with limited calcite cement. The three samples with little calcite cement (<5% calcite) have fairly low porosity owing to relatively abundant clay minerals (mainly kaolinite and illite; Table 1). These samples have a few per cent quartz cement (Fig. 8a, b). There is no evidence for the corrosion of detrital quartz grains (unlike in highly calcite cemented samples, see later). K-feldspar overgrowths can be

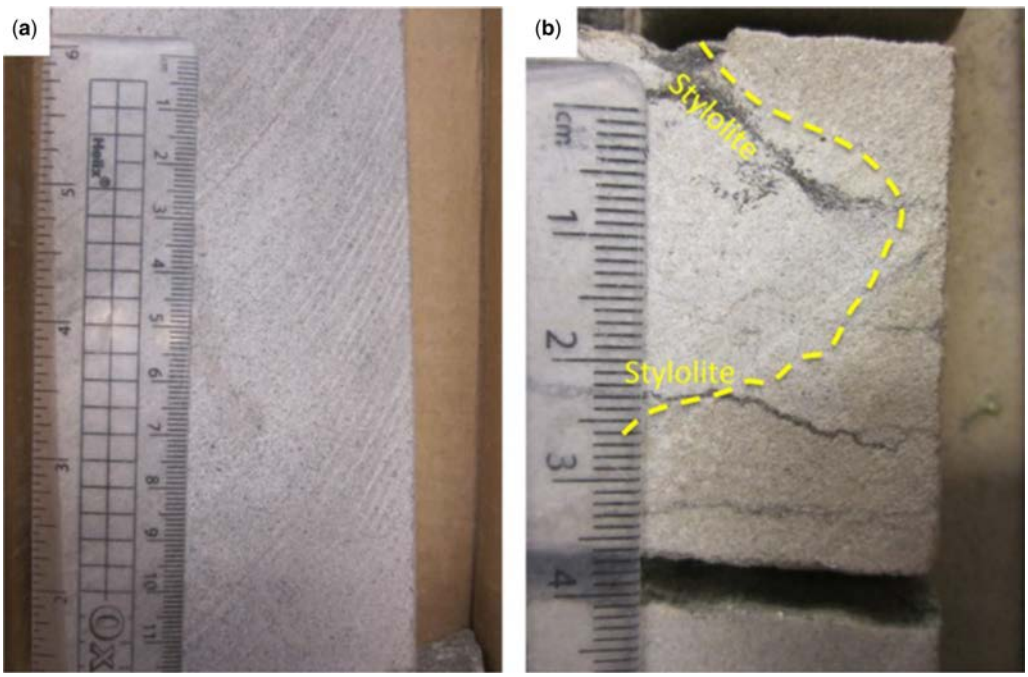

Fig. 7. (**a**) Core photograph of a strata-bound calcite-cemented horizon (well 2/5-2; 10789.5 ft) in the Brent Group of the Heather Field. Note the white/grey colour and pervasive nature of the calcite cement. (**b**) Core photograph of a centimetre-scale calcite nodule in the Brent Group of the Heather Field (well 2/5-2; 10820 ft). The dashed yellow line marks the boundary between the calcite nodule and the non-cemented portion of the reservoir. Note that the calcite cement also grows around stylolites.

discerned in these samples, but these overgrowths have undergone subsequent partial dissolution (Fig. 8b). Large, grain-sized patches of kaolinite possibly represent the complete dissolution and replacement of detrital plagioclase or K-feldspar grains (Fig. 8a, b). Minor pore-filling pyrite is present in these samples, much of it framboidal. The samples with relatively small quantities of calcite cement have relatively low porosity (<12%) owing to a combination of compaction, quartz and K-feldspar cementation and the growth of clay minerals, kaolinite mainly, in pores. Small amounts of secondary porosity owing to feldspar dissolution are present (Fig. 8a, b).

Samples with abundant calcite cement. Calcite-cemented zones have a loosely packed 'floating grain' texture, and localized point-to-point grain contacts (Figs 9a–d & 10a–d). Most calcite cement occurs as large, pokilotopic crystals (several millimetres in length and width) that host numerous detrital grains and that obliterate porosity. Calcite cement also occurs as a finer-grained mosaic of anhedral crystals (up to 20 μm in diameter). Gradation from mosaic to poikilotopic crystals occurs, although poikilotopic calcite is dominant. Calcite fills intergranular pore space, but it also fills secondary dissolution features in K-feldspar grains and overgrowths and fractures within quartz grains (Fig. 9a, d). Calcite cement also encloses other authigenic phases, including K-feldspar overgrowths, vermiform kaolinite, illite, pyrite and quartz cement (Figs 9 & 10) indicating that at least some calcite cementation crystallized after the growth of these authigenic phases. K-feldspar overgrowths, locally surrounded by calcite cement (Fig. 10c), have euhedral crystal faces, suggesting that they grew into open pores with no competition for space. Compactional features such as stylolites, minor pressure solution features between grains and splayed muscovite are enclosed by calcite cement. Replacement of detrital K-feldspar grains by calcite and kaolinite is evident, but detrital quartz grains are also corroded and embayed in calcite-rich samples (Figs 9a–d & 10a–d).

Point count analysis revealed that calcite-cemented zones have approaching 40% intergranular volume (minus-cement porosity; Table 1). There is an inverse relationship between calcite cement and detrital quartz, suggesting either that quartz-poor samples have been preferentially calcite-cemented or calcite has replaced quartz (Fig. 11a). There is an inverse relationship between calcite cement content and clay mineral content, suggesting that the

Table 1. *Point count data for the 19 Heather Field samples with careful differentiation of pore-filling and grain- and cement-replacive cements to allow for accurate determination of compactional porosity-loss and cementational porosity-loss (CEPL) using methods outlined by Houseknecht (1987) and the assumption that the original porosity was 45% (Beard & Weyl 1973)*

Well name	Sample depth	Grain size, μm	Sorting (trask)	Monocrystalline quartz (%)	Polycrystalline quartz (%)	Detrital K-feldspar (%)	Extra-basinal clay-rich lithic (%)	Detrital muscovite (%)	Detyrirtal rutile (%)	Matrix clay (%)	Replacive calcite (%)	Intergranular porosity-filling calcite (%)
2/5_H1	10646.0	546	1.58	41.7	5.7	20.0	0.7	2.7	0.0	0.3	0.0	0.0
2/5_H1	10711.9	643	1.29	50.3	9.0	16.0	0.0	0.7	0.0	3.9	3.3	5.0
2/5_H1	10729.0	616	1.29	37.3	6.3	11.3	0.0	0.7	0.0	0.0	2.3	32.0
2/5_H1	10731.3	153	1.23	39.7	7.3	12.6	0.0	0.0	0.0	0.0	3.8	30.3
2/5_H1	10734.8	654	1.30	33.7	12.0	11.7	0.0	0.7	0.0	0.0	3.0	34.4
2/5_2	10820.0	217	1.26	29.0	6.0	17.7	0.0	2.3	0.0	1.0	3.3	28.0
2/5_2	10843.6	504	1.35	22.3	7.7	22.3	0.0	3.7	0.0	0.0	2.7	33.7
2/5_2	10861.0	574	1.32	44.0	6.0	16.0	0.0	0.3	0.0	0.0	0.0	3.4
2/5_2	10885.1	627	1.30	37.7	9.0	10.0	0.0	0.0	0.0	0.0	3.7	32.0
2/5_H18	11460.3	210	1.24	24.7	3.3	22.3	0.0	1.3	0.0	0.0	2.0	32.0
2/5_H18	11478.5	167	1.26	30.3	3.3	13.0	0.0	1.7	0.0	0.0	5.0	41.3
2/5_H18	11500.3	169	1.34	1.0	0.0	5.9	0.0	7.9	0.0	0.0	34.3	40.7
2/5_H18	11527.7	N/A	N/A	39.7	6.7	13.0	0.3	0.0	0.3	0.0	6.0	14.0
2/5_H18	11543.5	583	1.24	36.7	7.3	13.0	0.0	0.0	0.0	0.0	2.7	32.3
2/5_H2	11773.0	458	1.62	25.0	10.3	20.0	0.0	3.0	0.0	0.0	0.6	32.0
2/5_H2	11776.0	160	1.27	43.0	10.0	16.3	0.0	0.3	0.0	0.0	0.0	0.0
2/5_H2	11797.6	172	1.22	36.0	8.7	16.7	0.0	0.0	0.0	0.0	2.9	25.0
2/5_H2	11808.6	602	1.39	36.7	11.0	12.0	0.0	0.0	0.0	0.0	3.7	24.0
2/5_H2	11828.1	551	1.17	43.3	10.3	9.3	0.0	1.0	0.0	0.0	1.4	25.0

Well name	Fracture-filling calcite (%)	Intergranular porosity-filling chlorite (%)	Replacive chlorite (%)	Intergranular porosity-filling kaolinite (%)	Replacive kaolinite (%)	Intergranular porosity-filling illite (%)	Replacive illite (%)	Intergranular porosity-filling K-feldspar (%)	Replacive K-feldspar (%)	Intergranular porosity-filling pyrite (%)	Replacive pyrite (%)	Fracture-filling pyrite (%)
2/5_H1	0.0	0.0	0.0	7.3	0.3	1.3	2.7	4.7	0.3	1.7	0.0	0.0
2/5_H1	0.0	0.0	0.0	1.7	0.7	0.3	0.0	2.0	0.0	0.3	0.0	0.0
2/5_H1	0.0	0.0	0.0	2.3	0.0	0.3	1.3	1.7	0.0	0.3	0.3	0.0
2/5_H1	0.0	0.0	0.0	0.0	0.0	0.0	0.3	1.7	0.0	0.0	0.0	0.0
2/5_H1	0.0	0.0	0.0	1.7	0.0	0.0	0.0	0.3	0.0	0.3	0.0	0.0
2/5_2	0.0	0.0	0.0	2.0	0.3	0.0	0.7	2.6	0.0	2.0	0.7	0.7
2/5_2	0.0	0.0	0.0	0.3	0.0	0.0	0.3	4.0	0.0	1.3	0.3	0.0
2/5_2	0.0	0.7	0.0	7.7	0.0	3.0	3.3	1.6	0.0	2.7	0.0	0.0
2/5_2	0.3	0.0	0.0	2.0	0.3	0.0	1.3	1.3	0.0	1.0	0.0	0.0

2/5_H18	0.0	0.0	0.0	0.0	0.0	0.0	0.3	3.0	0.0	0.0	0.0	0.0
2/5_H18	0.0	0.0	0.0	0.0	0.3	0.0	0.0	1.3	0.0	0.0	0.0	0.0
2/5_H18	2.3	0.0	0.0	0.0	0.0	0.0	1.3	0.0	0.0	3.9	2.6	0.0
2/5_H18	0.3	0.7	0.3	0.0	0.0	0.7	1.6	1.3	0.0	8.0	0.7	0.0
2/5_H18	0.0	0.0	0.0	1.7	0.3	0.0	0.7	2.7	0.0	1.0	0.0	0.0
2/5_H2	0.0	0.0	0.0	0.0	0.0	0.0	0.3	4.7	0.0	0.0	0.0	0.0
2/5_H2	0.0	0.0	0.0	4.3	0.0	0.7	1.3	2.3	0.0	2.7	0.0	0.0
2/5_H2	0.0	0.0	0.0	0.7	1.0	0.0	1.3	3.7	0.0	1.0	0.6	0.0
2/5_H2	0.0	0.0	0.0	0.0	0.3	0.7	0.3	5.3	0.0	1.3	0.0	0.0
2/5_H2	0.0	0.0	0.0	0.7	0.0	0.3	0.7	2.7	0.0	1.3	0.0	0.0

Well name	Intergranular porosity-filling quartz (%)	Intergranular porosity (%)	Intragranular secondary porosity (%)	Fracture porosity (%)	Intercrystalline porosity (%)	Microporosity (%)	Undifferentiated porosity (%)	Calculated cement volume (%)	Calculated intergranular volume (%)	Original porosity destroyed by compaction (COPL) (%)	Original porosity destroyed by cemenation (CEPL) (%)	Total porosity loss (%)
2/5_H1	3.6	2.3	3.3	0.0	0.0	0.6	0.3	18.6	20.9	53.6	41.3	65.4
2/5_H1	2.0	1.3	1.6	0.0	0.0	1.3	0.0	11.3	12.6	72.0	25.1	57.5
2/5_H1	1.3	0.3	1.0	0.0	0.0	0.6	0.3	37.9	38.2	15.1	84.2	91.0
2/5_H1	1.0	0.0	1.0	0.0	0.0	0.0	0.0	33.0	33.0	26.7	73.3	85.3
2/5_H1	1.3	0.0	0.3	0.0	0.6	0.0	0.0	38.0	38.0	15.6	84.4	91.4
2/5_2	2.7	0.0	0.3	0.7	0.0	0.0	0.0	37.3	37.3	17.1	82.9	90.6
2/5_2	1.3	0.0	0.0	0.0	0.0	0.0	0.0	40.6	40.6	9.8	90.2	94.6
2/5_2	2.3	4.0	3.9	0.0	0.0	0.7	0.0	21.4	25.4	43.6	47.6	67.2
2/5_2	0.7	0.0	0.0	0.0	0.3	0.0	0.0	37.0	37.0	17.8	82.2	90.2
2/5_H18	3.7	0.0	0.0	0.0	0.0	0.0	0.0	38.7	38.7	14.0	86.0	92.3
2/5_H18	0.3	0.3	0.0	0.7	0.0	0.0	0.0	42.9	43.2	4.0	95.3	97.1
2/5_H18	0.0	0.0	0.0	0.0	0.0	0.0	0.0	44.6	44.6	0.9	99.1	99.5
2/5_H18	3.0	1.0	1.7	0.0	0.0	0.3	0.0	27.7	28.7	36.2	61.6	77.9
2/5_H18	0.6	0.0	0.3	0.0	0.0	0.6	0.0	38.3	38.3	14.9	85.1	91.8
2/5_H2	1.7	1.0	0.0	0.0	0.0	0.0	0.0	38.4	39.4	12.4	85.3	90.9
2/5_H2	3.0	12.3	2.3	0.0	0.0	0.0	0.3	13.0	25.3	43.8	28.9	48.6
2/5_H2	0.3	0.7	0.3	0.0	0.0	0.0	0.0	30.7	31.4	30.2	68.2	81.8
2/5_H2	1.0	0.3	1.0	0.0	0.3	2.0	0.0	32.3	32.6	27.6	71.8	84.2
2/5_H2	2.6	0.3	0.0	0.0	0.0	0.7	0.3	32.6	32.9	26.9	72.4	84.5

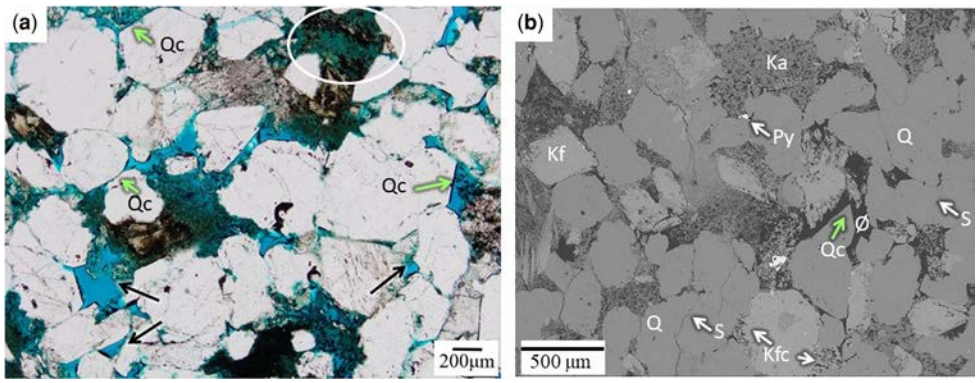

Fig. 8. Images of poorly calcite cemented sample from well 2/5-H1 (10,646.0 ft). (**a**) Light optical image showing the lack of calcite cement, the coarse grain size of this sandstone and the presence of primary porosity revealed by the blue-dyed resin. K-feldspar dissolution (white circle at the top) was followed by the precipitation of kaolinite. Minor quantities of quartz cement (Qc) are present (green arrows). (**b**) BSEM image showing the dominance of detrital quartz (Q) and K-feldspar (Kf) in these sandstones. There are sutured contacts (S) between quartz grains owing to the presence of grain-grain stylolites (S). There are large patches of kaolinite (Ka) that have probably replaced detrital K-feldspar. K-feldspar cement (Kfc; white arrow) grew directly on detrital K-feldspar but the K-feldspar cement then underwent dissolution. Quartz cement (Qc) is present (green arrow). Minor pyrite is present (Py).

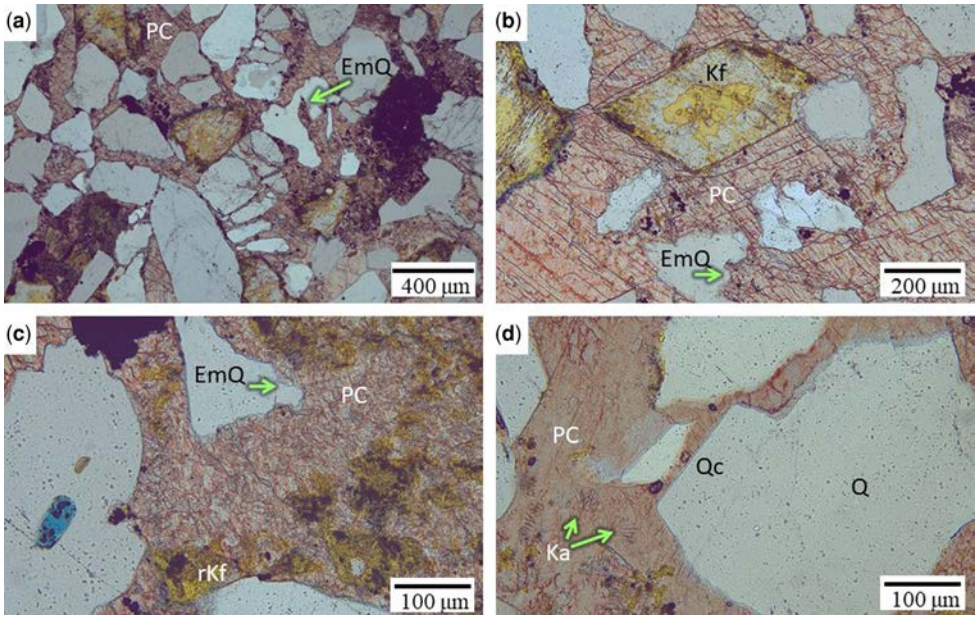

Fig. 9. Light optical photomicrographs of calcite-cemented Heather samples. (**a**) 2/5-H1 10,731.3 ft, no remaining primary porosity owing to poikilotopic calcite cement (PC) with isolated and embayed detrital quartz grains (EmQ) and quartz grains with highly irregular outlines. There are few grain–grain contacts resulting in a 'floating grain' texture. (**b**) 2/5-H1 10,731.3 ft, no remaining primary porosity owing to poikilotopic calcite cement (PC) with embayed detrital quartz grains (EmQ); yellow-stained detrital K-feldspar (Kf) has a euhedral outline suggesting that K-feldspar overgrowth grew before calcite filled the pore space. (**c**) 2/5-H1 10,731.3 ft, 2/5-H1 10,731.3 ft, no remaining primary porosity owing to poikilotopic calcite cement (PC) filling a secondary pore owing to the dissolution of detrital K-feldspar (note the remnant yellow stained K-feldspar within the pore-filling calcite). (**d**) 2/5-H18 11,543.5 ft, no remaining primary porosity owing to poikilotopic calcite cement (PC) that grew after quartz cement (Qc), note the euhedral outline to the large quartz (Q) grain. Kaolinite booklets (Ka) have been surrounded by later pore-filling calcite.

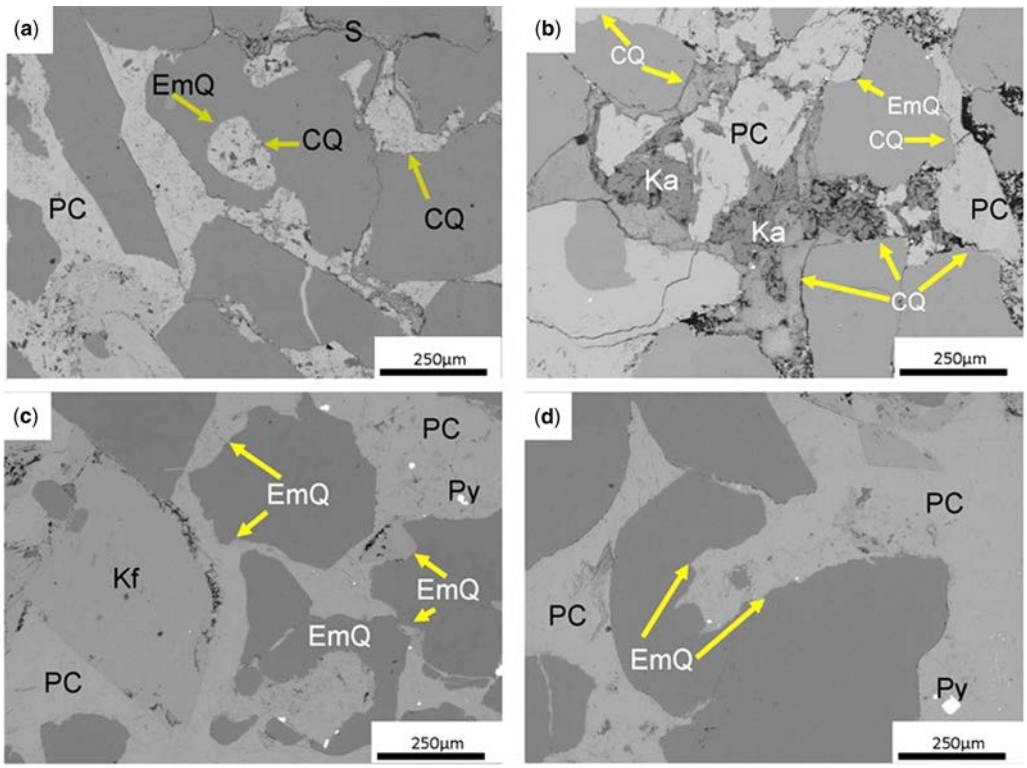

Fig. 10. (a–d) B-SEM images of corroded (CQ) and embayed (EmQ) quartz grains, and replacive nature of calcite cement (PC). Stylolites (S) are also visible. Calcite cement encloses pyrite (Py) and pore-filling kaolinite (Ka). Quartz grains appear embayed (EmQ) and corroded (CQ). (**a**) Sampled from well 2/5-H1; 10711.75 ft. (**b**) Sampled from well 2/5-H2; 11808.58 ft. (**c**) Sampled from 2/5-H18; 11543.42 ft. (**d**) Sampled from 2/5-H18; 11543.42 ft.

cleanest samples have been preferentially cemented with the carbonate (Fig. 11b). Point count data have been used to create a diagram to assess the dominant controls on porosity loss using the approach described by Houseknecht (1987). A diagram showing intergranular volume and cement volume (Fig. 12)

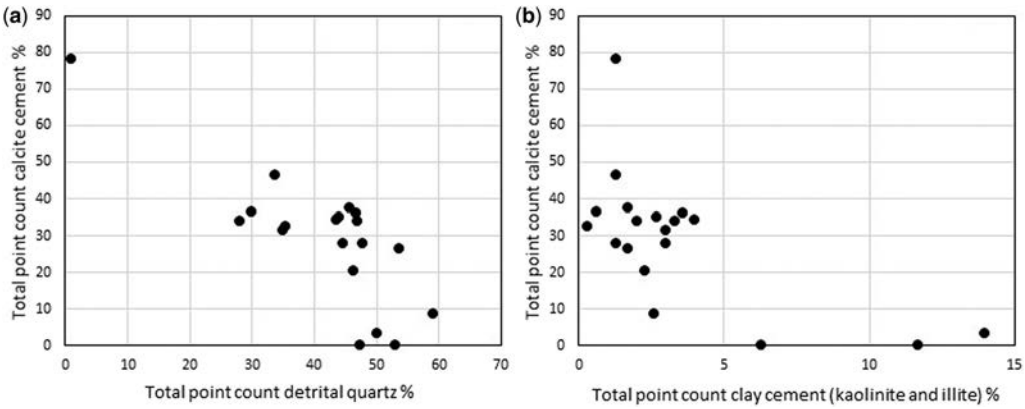

Fig. 11. Point count data from all 19 samples. (**a**) Comparison of total authigenic calcite and detrital quartz. Samples with greater quantities of authigenic calcite have lower quantities of detrital quartz. (**b**) Comparison of total authigenic calcite and authigenic kaolinite and illite. The most clay-rich samples have the lowest quantities of authigenic calcite.

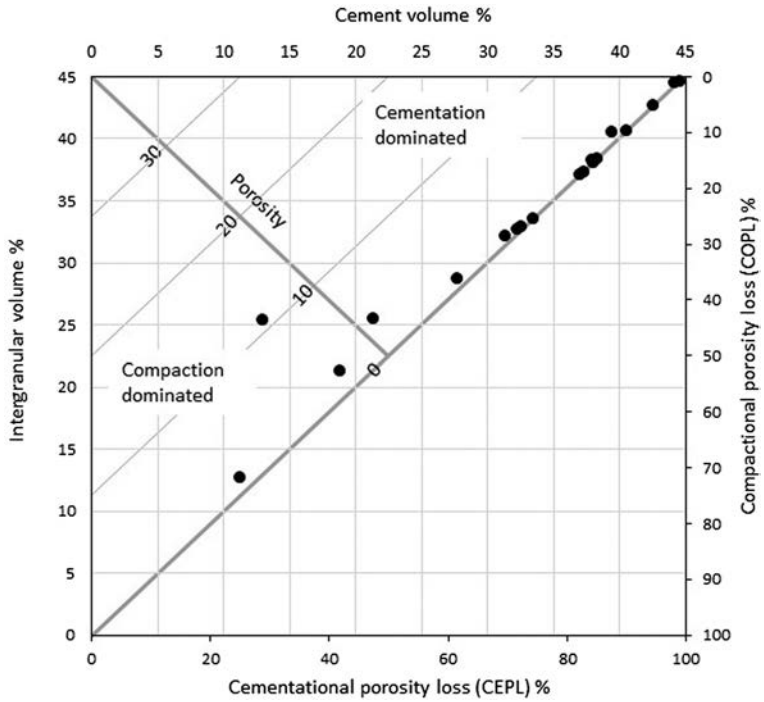

Fig. 12. Point count data of the variably calcite cemented samples from the Heather Field presented as a compaction v. cementation diagram (Houseknecht 1987). Most of the samples studied have low visible porosity (Table 1) so it is not surprising that most data lie on, or close to, the 0% isoporosity line. Almost all samples studied lie in the area representing cementation-dominated rocks (upper triangular area). The one exception that lies in the compaction-dominated area (left triangular are) well 2/5-H1, 10711.9 ft) is the most matrix-rich sample that has relatively little calcite cement (8%), suggesting that depositional matrix has exacerbated compaction and inhibited calcite cementation.

shows that most samples have porosity loss dominated by cementation.

SEM-EDS data

SEM-EDS analysis confirmed that calcite cement occurs in a wide range of abundances from 0 to 79% (Figs 13 & 14, Table 2). Apart from the outlier with nearly 79%, there is a cluster of samples that contains between 30 and 40% calcite, consistent with data from conventional petrographic techniques (Table 1). Quartz, K-feldspar and muscovite are the dominant detrital minerals (Figs 13 & 14). Calcite tends to occur as fully cemented patches (Fig. 14b) of various sizes (millimetres to centimetres at the SEM-EDS scale but up to metres, as seen in core: Fig. 7). The samples with minor calcite cement reveal detrital quartz and K-feldspar and small quantities of quartz cement as well as pre-filling kaolinite and illite (Fig. 14c). SEM-EDS analysis revealed a negligible quantity of plagioclase feldspar throughout the Heather succession. The part of Figure 14 that contains abundant calcite confirms the floating detrital grain structure evident in Figures 9 and 10 in which grains appear to be unusually separated from each other (Fig. 14b). The calcite cemented areas also contain embayed quartz grains and patches of rock in which quartz appears to have been largely dissolved out (Fig. 14b).

The core sample with 79% calcite (Fig. 15) has an unusual texture with strongly aligned micas that reflect primary bedding. Quartz grains have been preferentially dissolved leaving remnants of detrital quartz floating in diagenetic calcite. K-feldspar grains seem to be more intact than quartz grains, resulting in nearly three times as much remaining detrital K-feldspar as detrital quartz (Table 2); this suggests that the rock is a diagenetic product of the replacement of silicate grains by calcite. To emphasize this point, the sample imaged in Figure 15 is the result of mass dissolution of detrital quartz with relatively less dissolution of K-feldspar, before or during calcite precipitation. This sample, and its evidence of bulk quartz dissolution, confirms the dissolution origin of the commonly embayed quartz grain textures within calcite cemented volumes of the

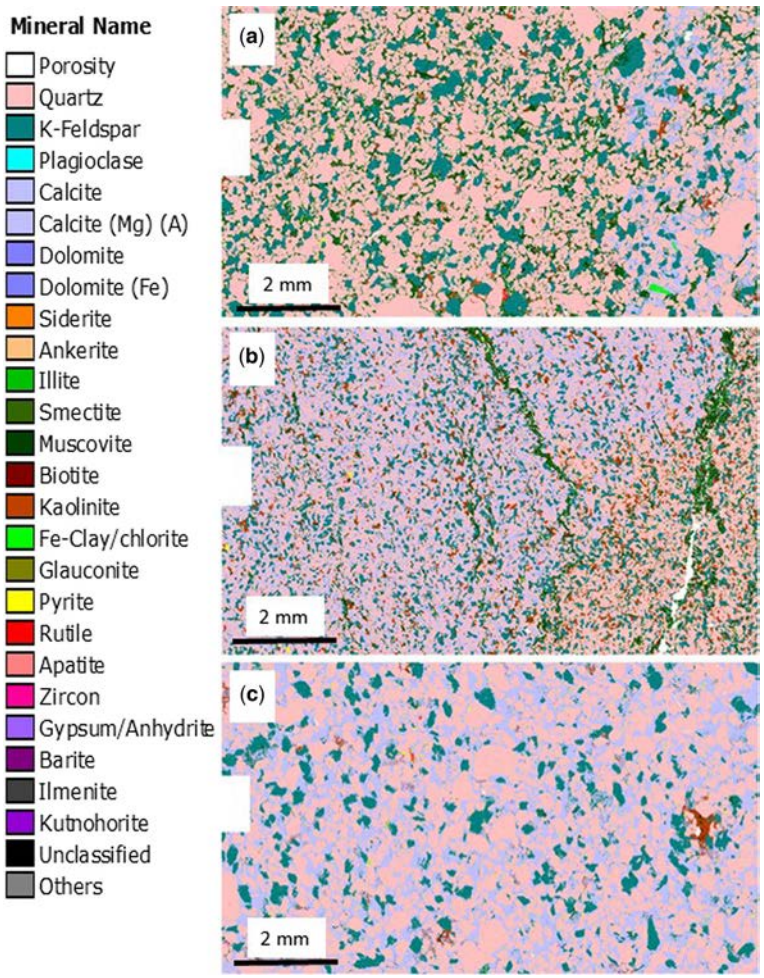

Fig. 13. SEM-EDS mineralogy images of variably calcite-cemented horizons from the Broom Formation in the Brent Group of the Heather Field (**a**, 2/5-H1, 10711.9 ft 5.57% calcite; **b**, 2/5-2, 10820.0 ft 38.29% calcite; **c**, 2/5-H1, 10731.3 ft 35.23% calcite; **d**, 2/5_H18, 11500.3 ft 78.96% calcite). Calcite locally occludes porosity. Intergranular volumes (minus cement porosities) of 30–40%, loose apparent grain packing and floating to point grain contacts are evident. Quartz is the dominant detrital minerals in many highly calcite-cemented zones with subordinate K-feldspar

Heather Field recorded using light optics (Fig. 9) and BSEM (Fig. 10).

The SEM-EDS data confirm the point count data (Fig. 11a), revealing an inverse relationship between calcite and quartz (Fig. 16a). This supports the observation that quartz has dissolved and been lost from the calcite-cemented parts of the rock. The same conclusion can be drawn for K-feldspar since it, too, has lower concentrations with increasing calcite (Fig. 16b). There is also a crude inverse relationship between calcite content and clay mineral content (and see Fig. 11b), suggesting that the cleanest samples have been preferentially cemented with the carbonate (Fig. 16c).

Stable isotope data

The stable isotope data from calcite cement, both newly produced during this study (Table 2) and from previous publications (Glasmann *et al.* 1989*b*), represent a significant range (Fig. 18). Calcite $\delta^{18}O$ values vary from −13.12 to −9.03‰ VPDB, with an average of −10.46‰ VPDB. Calcite $\delta^{13}C$ values vary from −30.57 to −3.18‰ VPDB, with an average of −12.68‰ VPDB; the range of calcite $\delta^{13}C$ values is typical of Brent Group data reported from the North Sea (Macaulay *et al.* 1998). There is no simple relationship between the amount of calcite and carbon or oxygen isotope

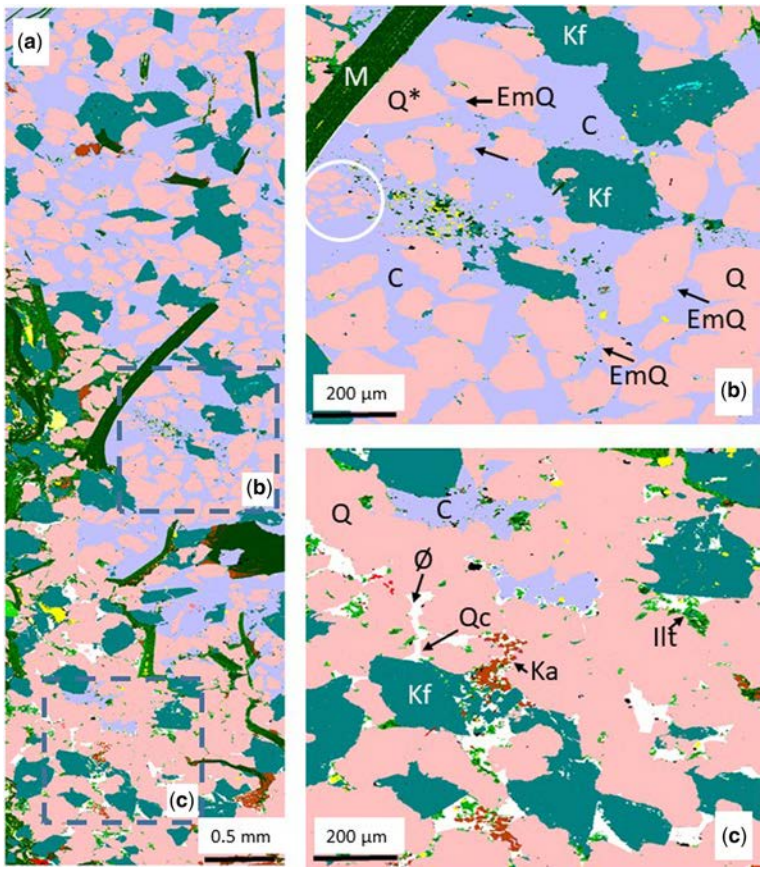

Fig. 14. SEM-EDS mineralogy images of heterogeneously calcite-cemented horizon from the Broom Formation in the Brent Group of the Heather Field, well 2/5-H18 (11460.3 ft). (**a**) The lower left part of the image has little calcite cement; the upper and lower right part of the image is extensively calcite cemented. Parts b and c are enlarged part of the left-hand image (a). (**b**) This shows details of the calcite cemented part of this sample. Pore-filling calcite (C) surrounds detrital quartz (Q), K-feldspar (Kf) and mica (M). Detrital quartz seems to have a rather embayed outline (EmQ) including a patch of quartz grains that seem to represent the breakdown of an earlier silicate grain (white oval). The mica flake has been abutted by a quartz grain (Q*), which has an unusually straight edge with the mica. This may represent pressure solution of the quartz grain against the mica (Bjørkum 1996), suggesting that the pore-filling calcite developed after quartz–mica pressure solution. (**c**) This shows details of the more porous (Ø) part of the sample with a small amount of pore-filling calcite, as well as pore-filling clay minerals: kaolinite (Ka) and Illite (Ilt). Localized quartz cement (Qc) is revealed by euhedral outlines.

values (Fig. 19). However, the smaller volumes of calcite tend to have less negative $\delta^{13}C$ values and the unusual sample with 79% calcite (effectively a diagenetic limestone: Fig. 15) has one of the highest $\delta^{18}O$ values.

Fluid inclusion petrography and microthermometry

Calcite was easily identified in the fluid inclusion wafers based upon its location in the pore network relative to grains and its white fluorescence when subject to UV light. Primary two-phase (liquid and vapour) aqueous fluid inclusions (up to 15 µm in length) are abundant (Fig. 20a, b). They appear as both isolated inclusions and in assemblages. Fluid inclusion microthermometry was undertaken on primary aqueous inclusions. Homogenization temperatures of secondary aqueous inclusions, such as those along healed fractures, were not measured because these signify events that occurred later than the original calcite phase of cementation. All data were collected from unfractured, pore-filling calcite as subsequent deformation of the fluid inclusion host can lead to alteration of homogenization temperatures (Worden *et al.* 1995), for example

Table 2. *Stable isotope and SEM-EDS mineralogy data for the 19 Heather Field samples*

Well name	Depth (ft)	$\delta^{13}C_{VPDB}$	$\delta^{18}O_{VPDB}$	Porosity	Quartz	K-Feldspar	Plagioclase	Calcite	Illite	Muscovite	Biotite	Kaolinite	Fe-Clay/ chlorite	Pyrite	Rutile	Apatite	Zircon	Others
2/5_H1	10646.0	−5.40	−10.94	2.87	49.89	25.57	0.01	0.00	1.72	6.88	0.05	13.30	0.03	0.39	1.53	0.19	0.02	0.43
2/5_H1	10711.9			2.17	61.36	17.88	0.05	5.68	3.21	8.93	0.04	2.32	0.08	0.20	0.08	0.02	0.00	0.14
2/5_H1	10729.0			0.24	50.48	11.38	0.20	35.07	0.33	0.51	0.02	1.32	0.01	0.41	0.01	0.15	0.01	0.10
2/5_H1	10731.3	−20.01	−10.01	0.46	49.96	11.99	0.11	35.40	0.34	0.33	0.01	1.15	0.00	0.59	0.03	0.02	0.00	0.08
2/5_H1	10734.8	−12.34	−9.70	0.53	50.17	12.77	0.10	33.87	0.39	0.46	0.01	1.81	0.00	0.24	0.06	0.05	0.00	0.05
2/5_2	10820.0	−26.39	−10.22	0.12	36.27	21.26	0.06	38.54	0.69	1.64	0.10	0.69	0.00	0.47	0.19	0.04	0.00	0.05
2/5_2	10843.6	−30.57	−10.23	0.12	36.27	21.26	0.06	38.54	0.69	1.64	0.10	0.69	0.00	0.47	0.19	0.04	0.00	0.05
2/5_2	10861.0	−11.77	−9.15	7.37	61.86	21.20	0.04	3.75	3.02	2.60	0.05	5.65	0.13	1.23	0.05	0.12	0.01	0.27
2/5_2	10885.1	−11.84	−9.28	0.42	49.37	14.49	0.16	31.91	0.44	0.46	0.01	2.40	0.00	0.13	0.04	0.50	0.00	0.09
2/5_H18	11460.3	−9.76	−9.42	0.10	40.50	19.05	0.23	30.94	0.80	1.89	0.07	5.33	0.05	0.24	0.68	0.09	0.02	0.12
2/5_H18	11478.5	−17.35	−10.06	0.25	44.01	12.21	0.17	40.30	0.56	0.97	0.04	1.18	0.00	0.21	0.19	0.06	0.00	0.08
2/5_H18	11500.3	−11.47	−9.08	0.04	2.24	6.51	0.30	79.12	2.53	4.10	0.32	2.72	0.02	1.79	0.12	0.11	0.00	0.12
2/5_H18	11527.7	−11.93	−13.12	2.84	50.59	21.58	0.04	17.54	0.83	0.92	0.10	0.22	0.13	7.40	0.03	0.15	0.01	0.48
2/5_H18	11543.5	−12.40	−9.03	0.35	48.42	16.09	0.14	32.33	0.56	0.64	0.02	1.46	0.00	0.22	0.02	0.03	0.01	0.05
2/5_H2	11773.0	−11.34	−13.00	0.19	44.34	21.18	0.03	32.63	0.42	0.64	0.03	0.17	0.00	0.38	0.11	0.01	0.00	0.04
2/5_H2	11776.0			12.95	60.95	29.46	0.02	0.00	2.51	2.34	0.04	2.72	0.00	1.49	0.16	0.02	0.00	0.26
2/5_H2	11797.6	−3.18	−11.41	0.81	46.48	22.04	0.04	28.97	0.91	0.55	0.02	0.36	0.04	0.45	0.03	0.01	0.01	0.08
2/5_H2	11808.6	−3.92	−11.35	1.70	50.21	22.67	0.04	23.29	1.66	1.00	0.02	0.77	0.10	0.10	0.04	0.03	0.01	0.07
2/5_H2	11828.1	−3.19	−11.32	0.91	51.82	17.41	0.04	28.60	0.46	0.45	0.01	0.91	0.00	0.19	0.01	0.04	0.00	0.04

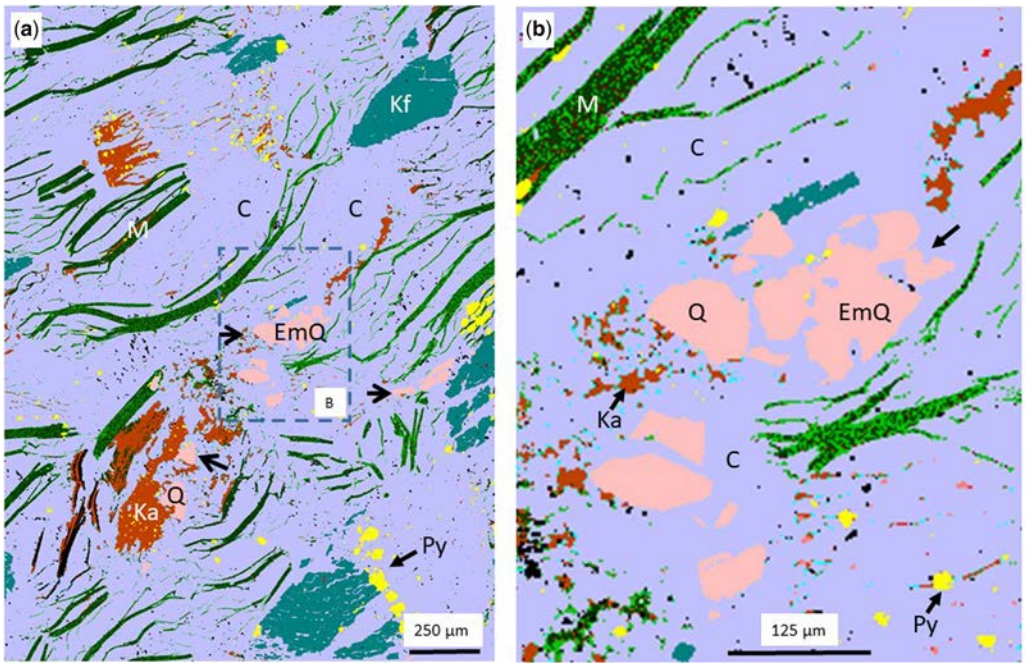

Fig. 15. SEM-EDS mineralogy images of heterogeneously calcite-cemented horizon from the Broom Formation in the Brent Group of the Heather Field, well 2/5-H18, 11500.3 ft. (**a**) This sample has an unusual mineralogy for a clastic rock with 79% calcite (C), 7%, K-feldspar (Kf), 4% muscovite (M), 2% quartz (Q) and 2% pyrite (Py). (**b**) Enlarged part of (a) showing details of remaining quartz, the absence of porosity and the primary bedding picked out by the micas. The quartz grains are heavily embayed (EmQ). The texture and mineralogy suggest that the rock is a diagenetic product of the replacement of silicate grains by calcite with major signs of preferential quartz dissolution (corroded grains arrowed), relatively abundant detrital mica (picking out the primary bedding) and significantly more remaining detrital K-feldspar than quartz.

fluid inclusions in calcite cemented fault zones are unlikely to reveal meaningful temperatures (Worden *et al.* 2016).

Fluid inclusion vapour to liquid ratios varied from 5:95 to 35:65. Aqueous two-phase inclusions exhibit elongate, euhedral and irregular shapes. Primary oil inclusions were identified by their white-blue fluorescence under UV illumination (Fig. 20c, d). Thermometric (phase) analysis was not carried out on oil inclusions, since the PVT properties of the oil in the inclusion are unknown.

A total of 93 two-phase aqueous inclusion homogenization temperatures (*Th*) were measured and display a range from 49.2 to 168.2°C (average of 90.3°C) (Fig. 21).

Discussion

Comparison of point count data and SEM-EDS mineralogy data

As the study used both point count data and SEM-EDS data, it is worth comparing these data (Fig. 17). Despite the totally different analytical approaches for the two techniques, porosity, quartz and calcite data correlate very well (Fig. 17a–c). K-feldspar correlates reasonably well but with more scatter (Fig. 17d). This may be due to slight under-recognition of K-feldspar during point counting, noting that the slope is considerably less than 1 (Fig. 17d). To the authors' knowledge this is the first published cross-comparison of point count and SEM-EDS data.

Stratigraphic distribution of calcite in the Heather Field

Throughout much of the Brent Province calcite is known to be a major pore-occluding cement that presents problems for both reservoir quality and compartmentalization. Calcite is commonly found in the lowermost Brent Group intervals of the marine Broom Formation (Fig. 5) (Walderhaug & Bjørkum 1992; Lundegard 1994; Girard 1998) and lower shoreface Rannoch Formation (Giles *et al.* 1992; Prosser *et al.* 1993). There is somewhat less calcite

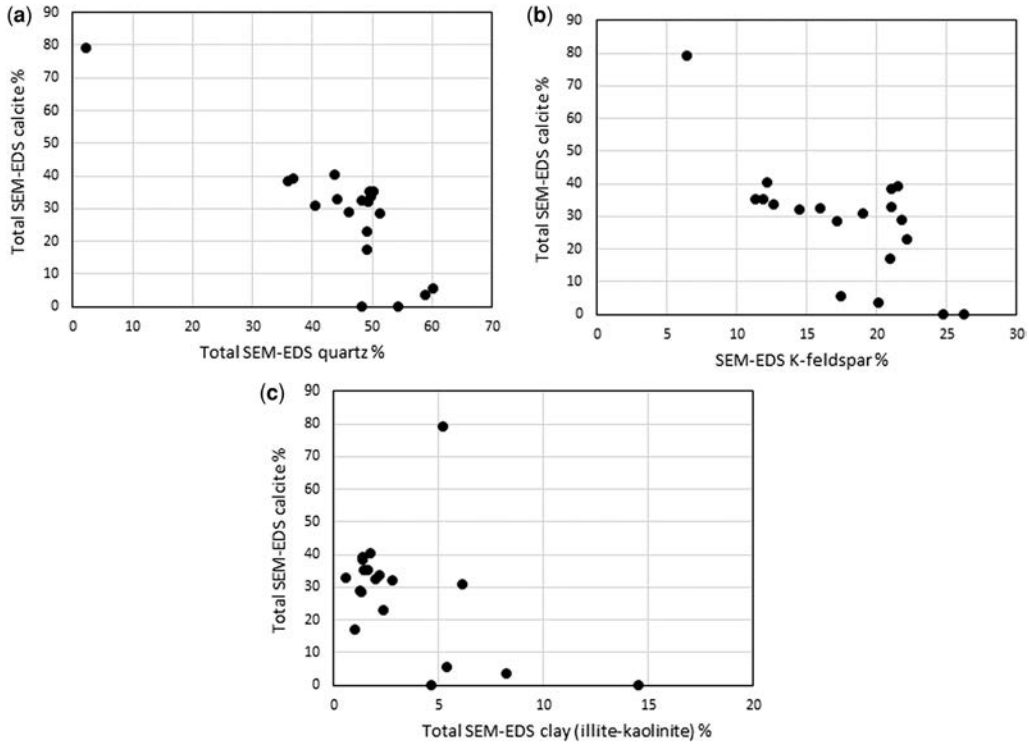

Fig. 16. SEM-EDS data from all 19 samples. (**a**) Comparison of calcite and quartz from data totalled to 100% including porosity. Samples with greater quantities of calcite have lower quantities of quartz. This is like the pattern derived from point count data (Fig. 11a). (**b**) Comparison of total calcite and total kaolinite and illite. The most clay-rich samples have the lowest quantities of calcite. This too is like the pattern derived from point count data (Fig. 11b). (**c**) Comparison of total calcite and K-feldspar. Samples with greater quantities of calcite have lower quantities of K-feldspar.

reported from the upper-shoreface and delta front sandstones of the Etive Formation, while the delta plain deposits of the Ness Formation are reported to have the least quantity of calcite (Bjørlykke *et al.* 1992; Giles *et al.* 1992). The marine transgressive sediments of the topmost Tarbert Formation locally contain abundant calcite cement (Lønøy *et al.* 1986; Girard *et al.* 2002) but have often been reported to be locally siderite cemented (Giles *et al.* 1992). The Brent Group sandstones deposited in marine environments thus tend to have more calcite cement than those deposited in fluvial-delta top environments (Scotchman *et al.* 1989; Bjørlykke *et al.* 1992).

Shallow marine sandstones routinely contain tightly calcite cemented intervals (Bjørkum & Walderhaug 1990*a*) with the calcite being demonstrated to be derived from bioclastic debris that was co-deposited with the primary clastic sediment in some cases (Bryant *et al.* 1988; Morris *et al.* 2006). The localization of calcite cement to the most marine parts of the Brent Group is unlikely to be coincidental. The abundance of calcite in Brent sandstones seems to be a direct function of depositional environment. Note that body fossils (shells fragments) are exceedingly rare in the Brent Group of the Heather Field; however they have been reported from the marine Broom Formation, including belemnites and bivalves (Walderhaug & Bjørkum 1992). Calcite-cemented layers within the Rannoch Formation were linked to the tops of shoaling-upwards marine cycles at which shell fragments would be expected to accumulate (Prosser *et al.* 1993). However, the reported rarity of direct evidence of calcareous shell debris has previously been assumed to be proof that calcite cementation was not related to the primary accumulation of bioclastic detritus (Glasmann *et al.* 1989*b*). Note that the absence of direct evidence of bioclasts or early (marine) cements does not prove that the pervasive calcite cement was not initially derived from marine bioclastic material, especially for a mineral that is relatively soluble (compared with silicate minerals). Some of the calcite cement may have been derived from an

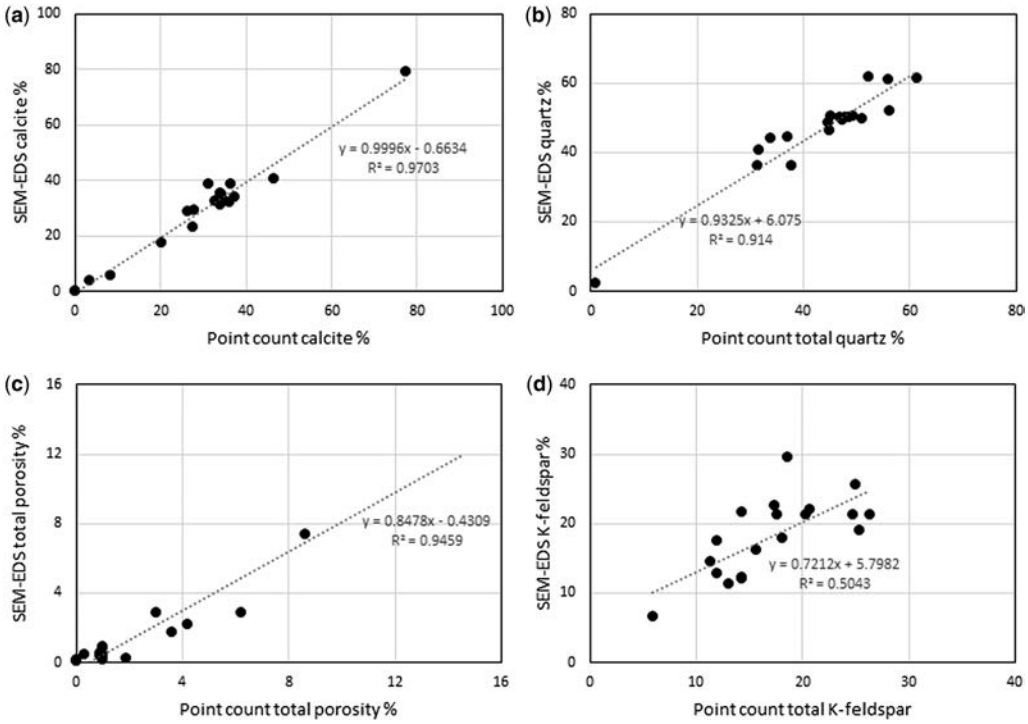

Fig. 17. Comparison of point count and SEM-EDS mineralogy and porosity. (**a**) Point count calcite v. SEM-EDS calcite revealing an excellent correlation. (**b**) Point count quartz v. SEM-EDS quartz revealing an excellent correlation. (**c**) Point count porosity v. SEM-EDS porosity revealing an excellent correlation. (**d**) Point count K-feldspar v. SEM-EDS K-feldspar revealing a moderate degree of correlation with the point count data somewhat under-estimating the amount of K-feldspar.

early, possibly aragonite, marine cement that developed soon after deposition (Vieira *et al.* 2007); note that such cement would not necessarily leave any textural evidence in the mesogenetic rock that resulted from the following 160 myr of history with heating to over 100°C. It is also possible that diagenetic calcite originated from detrital micritic, as opposed to coarse-grained, carbonate. Furthermore, note that there seem to have been numerous sources of dissolved CO_2 that would have been capable of creating low pH pore waters that could mobilize and redistribute the $CaCO_3$ bioclasts, micrite or marine cements; this will be addressed further when the carbon isotope data are considered.

Timing of calcite growth in the Heather Field

There is a range of clues available to help determine the timing of calcite growth including the high intergranular volume in calcite-cemented sandstone (Table 1; Fig. 12), the presence of corroded quartz grains in samples with abundant calcite (Figs 9, 10, 14 & 15), fluid inclusion homogenization data (Fig. 21), the presence of primary oil inclusions in calcite (Fig. 20) and complex relative growth relationships between calcite and other minerals such as kaolinite and quartz (Figs 9, 10 & 13–15).

Calcite commonly represents 30–40% of the total volume of the cemented parts of the Brent Group from Heather, listed here (Tables 1 & 2) and also reported by Glasmann *et al.* (1989*b*). High intergranular volumes of calcite have been routinely reported from calcite-cemented portions of the Brent Group (Bjørkum & Walderhaug 1990*a*, b; Bjørlykke *et al.* 1992; Giles *et al.* 1992; Prosser *et al.* 1993). The intergranular volume (cement plus remaining porosity) can be taken as an indication of timing of cement growth relative to compaction and can thus be used to interpret the relative timing of cement growth (Stephenson *et al.* 1992; Ehrenberg 1995; Dutton 1997). Given that most sandstones have about 40–45% porosity when they are deposited (Beard & Weyl 1973), the Heather Field reservoir sandstones having up to 40% calcite by volume suggests that growth happened before any burial-induced compaction had occurred. On this basis, it seems plausible to conclude that calcite growth happened during eodiagenesis, possibly very soon after deposition and

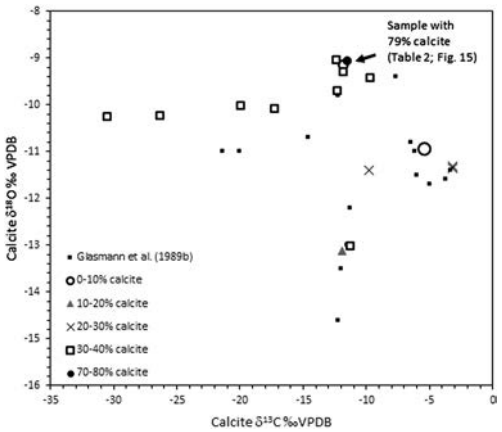

Fig. 18. δ^{18}O VPDB v. δ^{13}C VPDB for calcite cement of the Brent Group sandstones with new data from this study and data from the Broom Formation from the Heather Field from (Glasmann *et al.* 1989*b*). Calcite δ^{18}O values range between −13.12 and −9.03‰ VPDB; average of −10.46‰ VPDB. Calcite δ^{13}C values range between −30.57 and −3.18‰ VPDB; average of −12.68‰ VPDB. Variable δ^{13}C VPDB suggests a range of sources of the carbon in carbonate, although predominance for strongly negative δ^{13}C VPDB values is indicative of organic-derived carbon. Increasingly negative δ^{18}O VPDB values are indicative of calcite cementation with increasing temperature.

certainly before the first stages of mechanical compaction (grain rearrangement) had occurred (Worden *et al.* 2018*a*). On this basis, numerous authors have concluded that calcite growth in the Brent Group sandstones was an early phenomenon (Glasmann *et al.* 1989*b*; Giles *et al.* 1992; Prosser *et al.* 1993).

One sample that we examined had a mighty 79% calcite, with small amounts of K-feldspar, muscovite and trace amounts of quartz, kaolinite and pyrite (Fig. 15). However, the fabric displayed in this rock (Fig. 15) and the depletion of quartz relative to K-feldspar suggests that this rock is not simply a sandstone in which the detrital silicates were diluted by a large amount of calcite cement. Instead the elevated feldspar/quartz ratio suggests that quartz has been lost preferentially to other detrital minerals. Quartz grains in pervasively calcite-cemented Brent Group sandstones of the Heather Field locally have embayed (irregular and apparently pitted) outlines and have an open-packed, 'floating grain texture' (grains not seen in contact with each other, suggesting removal of the previous edges of quartz grains) (Figs 9–10 & 13–15). Similar open-packing textures and embayed and floating quartz grains have been reported previously for Brent Group sandstones (Lønøy *et al.* 1986; Saigal & Bjørlykke 1987; Prosser *et al.* 1993, 1994; Lundegard 1994) and were interpreted to represent the results of localized quartz dissolution. Note that the dissolution of quartz and other silicate grains during early carbonate diagenesis has been reported from other depositional environments including in calcrete and dolocrete accumulations that developed in continental clastic deposits (Spotl & Wright 1992; Spotl *et al.* 1993; Worden 1998; Worden & Matray 1998; Worden *et al.* 1999). An implication of the growth of calcite

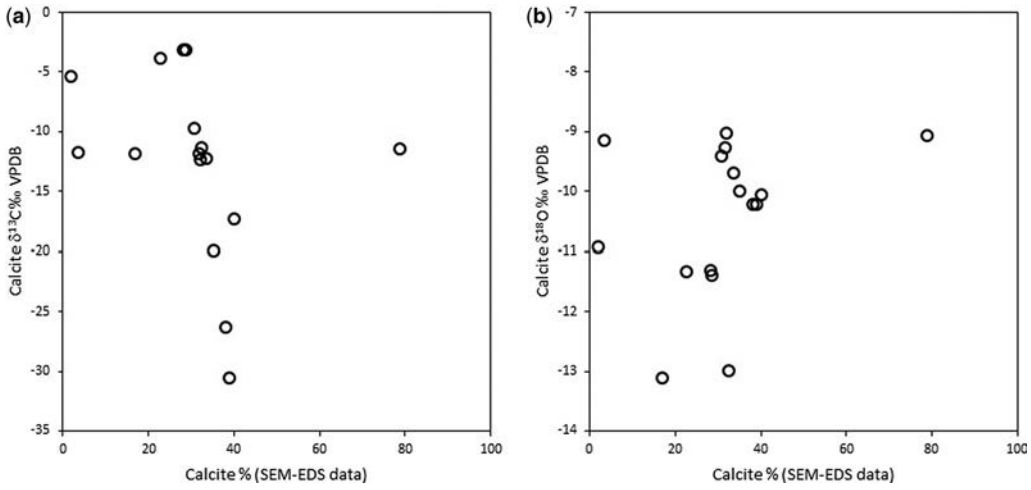

Fig. 19. SEM-EDS-derived amount of calcite v. (**a**) δ^{13}C VPDB and (**b**) δ^{18}O VPDB values from calcite from the Brent Group sandstones, Heather Field (this study). There is no simple relationship between the amount of calcite and its carbon isotope values, but smaller amounts tend to have less negative δ^{13}C values. Also, there is no simple relationship between the amount of calcite and oxygen isotopes, but it is noteworthy that the unusual sample with 78% calcite (Fig. 15) has one of the highest δ^{18}O values, possibly indicative of growth at relatively low temperature.

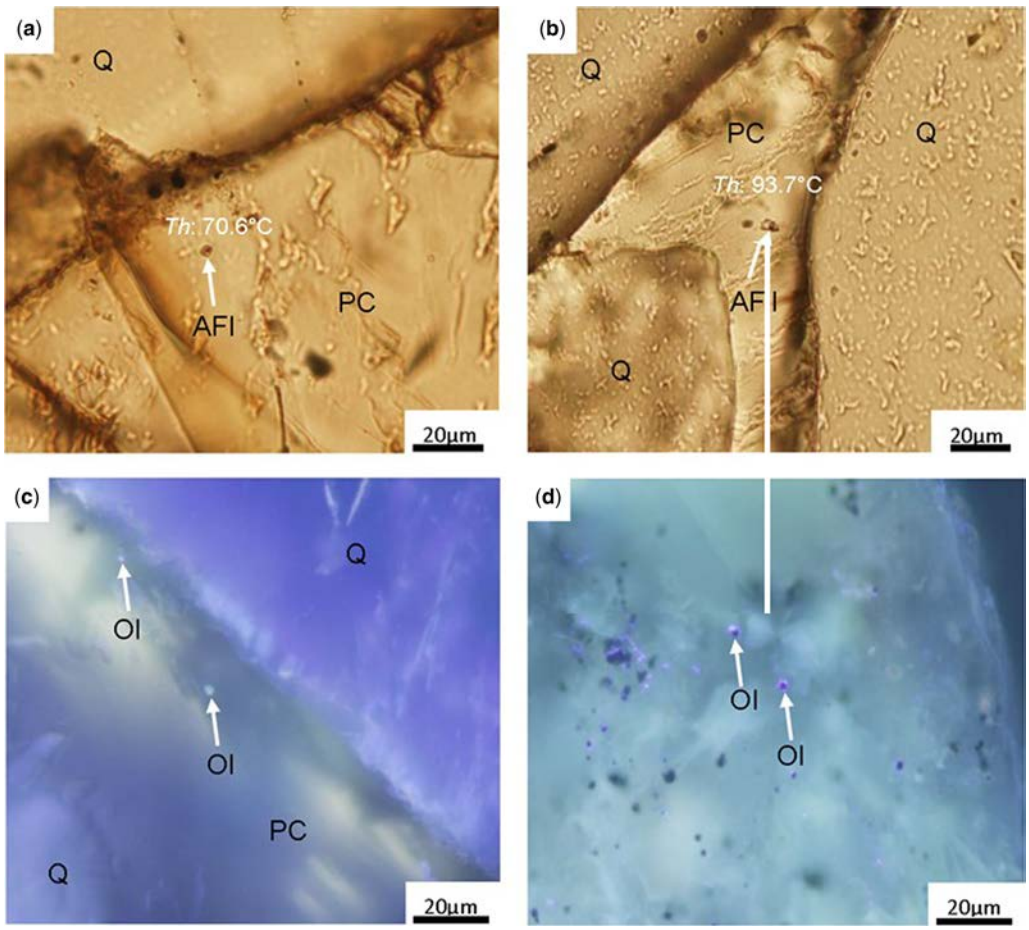

Fig. 20. (**a** and **b**) Representative images of aqueous primary two-phase fluid inclusions (AFI) in non-ferroan calcite (PC) (a, 2/5-H1, depth 10734.68 ft; b, 2/5-H18, depth 11543.42 ft). Homogenization temperatures, *Th*, suggest that a portion of the calcite cement is a high-temperature, deeper burial diagenetic phase. Note the euhedral shape of the inclusions. (**c** and **d**) Representative images of oil fluid inclusions (OI) in calcite cement (c, 2/5-2; depth 10885.08 ft; d, 2/5-H1, depth 10734.68 ft), showing their white-blue fluorescence under UV light. Their presence suggests that calcite cement grew during or after oil migration. Homogenization temperatures were not measured for oil inclusions. Quartz grains are marked with Q.

at the expense of detrital silicate grains is that intergranular volume measurements may lead to an underestimation of the depth of burial at the time of cementation, since some of the cement has replaced grains instead of just passively filling pores.

There is good petrographic evidence that at least some of the calcite cement developed later than kaolinite in the sequence of diagenetic events: calcite surrounds kaolinite booklets in some samples (Fig. 9d), suggesting that some calcite grew at temperatures higher than those interpreted for kaolinite growth, i.e. 45–60°C (Glasmann *et al.* 1989*b*), 54–75°C (Prosser *et al.* 1993), <45°C (Giles *et al.* 1992). Even more significant, calcite also surrounds quartz cement in a small number of samples (Fig. 9d) with quartz growth interpreted to be at temperatures greater than 80°C for most sandstones (Walderhaug *et al.* 2000), including those from the Brent Group (Bjørlykke *et al.* 1992; Hogg *et al.* 1992; Girard *et al.* 2001, 2002). On this basis, it is possible to conclude that at least some of the calcite in the Brent Group of the Heather Field grew at temperatures greater than 80°C.

The analysis of primary aqueous fluid inclusions from calcite revealed a range of homogenization temperatures greater than about 50°C, with a mode between 90 and 100°C (Fig. 21). The lack of homogenization temperatures lower than 50°C is not

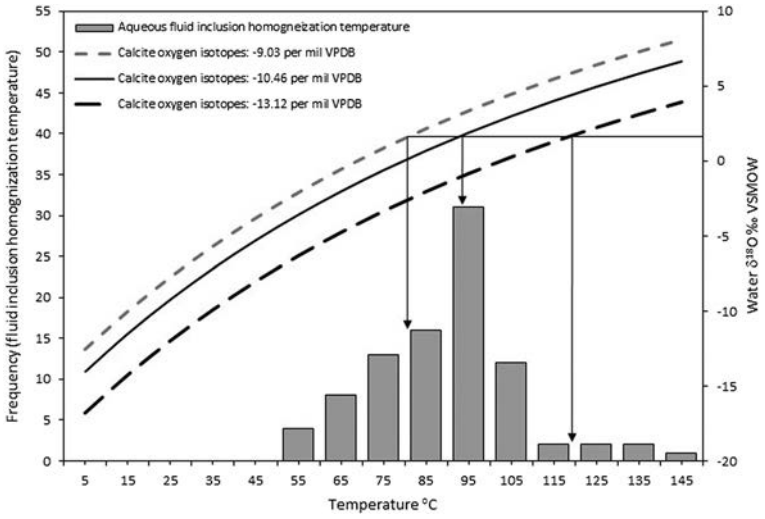

Fig. 21. Histogram of two-phase aqueous inclusion homogenization temperatures, *Th*, and a cross-plot of formation water δ^{18}O v. derived temperature for a range of calcite δ^{18}O values using the calcite–water oxygen isotope fractionation equation in Friedman & O'Neil (1977). The average *Th* value is 90.4°C with a range between 49.2 and 150°C. If the present day formation water oxygen isotopic composition of a typical Brent Province oil field (e.g. 2‰ VSMOW from the nearby Hild Field) (Warren & Smalley 1994) is compared with the maximum, mean and minimum calcite–water fractionation curves, it reveals that a proportion of the calcite cement grew in the temperature range of around 80 to about 125°C. This analysis suggests that a significant proportion of the calcite cement crystallized relatively late in the diagenetic sequence.

surprising since low-temperature inclusions seldom result in two-phase inclusions that can be used for homogenization measurements (Goldstein & Reynolds 1994). The mode at 90–100°C confirms the petrographic observations, and presents conclusive proof that at least some calcite growth, or recrystallization, occurred late in the diagenetic sequence. Similarly high-temperature aqueous fluid inclusions from calcite in Brent sandstones have been reported previously (Girard 1998; Girard *et al.* 2002), suggesting that this is not a phenomenon isolated to the Heather Field.

Primary oil-filled inclusions have also been found in calcite cement from Heather (Fig. 20). Apparently typical of the Brent province (Scotchman *et al.* 1989), oil filling was reported to have occurred relatively late in the burial history (Glasmann *et al.* 1989*b*) (25–20 Ma, Fig. 2). This suggests that at least some calcite precipitation has occurred within the last 25 myr. Primary oil-bearing inclusions in calcite were previously reported from the Broom-equivalent from the Oseberg field (Girard 1998), again suggesting that late growth or reprecipitation of calcite is not unique to the Heather Field.

The range of reported calcite oxygen stable isotope data (Table 2, Fig. 18) can be used to infer high calcite growth temperature if it grew in isotopic equilibrium with the present day formation water (Fig. 21) (Girard 1998). However, such an interpretation is open to counter arguments if calcite is assumed to have grown from meteoric water (see section on pore waters present during calcite growth). Consequently, the calcite δ^{18}O data will not be used as prima facie evidence of the temperature of calcite growth.

Overall, there are conflicting lines of evidence about the timing of calcite growth. There is evidence to suggest that some of the calcite may have formed early during eodiagenesis, especially the high intergranular volume and the lack of compaction fabrics in pervasively calcite cemented samples. Other lines of evidence prove that some of the calcite grew late in the history of these rocks during mesodiagenesis: calcite growth demonstrably later than kaolinite and quartz cement, high aqueous fluid inclusion homogenization temperatures and the presence of oil-filled primary inclusions within calcite. The distribution of aqueous fluid inclusion homogenization temperatures (Fig. 21) can be used to infer that calcite grew over a wide range of temperatures. It seems likely that some calcite formed soon after deposition and then calcite growth, or recrystallization, continued through to the last few (*c.* 25) million years. Note that the interpretation that calcite in the Brent Group is both eogenetic and mesogenetic was also reached by Giles *et al.* (1992), Bjørlykke *et al.* (1992) and Girard *et al.* (2002).

Pore waters present during calcite growth

The oxygen stable isotope ($\delta^{18}O$) value of any mineral is a function of the oxygen isotope value of the water from which the mineral grew and the temperature of mineral growth, assuming isotopic equilibrium between the mineral and the host water (Morad *et al.* 2003). If the mineral and formation water $\delta^{18}O$ values are known, then the growth temperature can be inferred. Calcite $\delta^{18}O$ values are shown in Figure 18 and listed in Table 2.

Virgin-produced formation water $\delta^{18}O$ data derived from drill stem tests from the Brent, from the nearby Hild Field, revealed that the present-day formation water has an oxygen isotopic composition of around 2‰ VSMOW, which is typical of the Brent Group (Warren & Smalley 1994). Such formation water $\delta^{18}O$ values represent water that has evolved, at relatively high temperature, in a geochemically closed system, i.e. not a system that has experienced major influx of water deep into a sedimentary basin (Morad *et al.* 2003).

Using the reported formation water $\delta^{18}O$ value from the Hild Field–Brent Group in conjunction with the calcite $\delta^{18}O$ data and the calcite–water isotope fractionation equation (Friedman & O'Neil 1977) suggests that calcite cementation occurred at temperatures between 80 and 125°C for calcite with $\delta^{18}O$ values ranging from −9.0 to −13.1‰ VPDB (Fig. 21). The intersection between the virgin formation water $\delta^{18}O$ data and the modelled calcite–water oxygen isotope equilibrium curves can be usefully compared with the aqueous inclusion homogenization temperature distribution. The modal homogenization temperature value (90–100°C) coincides with the average calcite $\delta^{18}O$ value of −10.5‰ VPDB (Fig. 21), thus seeming to support an interpretation of high-temperature (mesogenetic) calcite growth from a relatively closed system.

Note that a similar range of calcite $\delta^{18}O$ values has been previously used to infer growth of calcite from Mesozoic (late Jurassic to earliest Cretaceous) meteoric water with a water $\delta^{18}O$ value of about −8‰ VSMOW (Saigal & Bjørlykke 1987; Glasmann *et al.* 1989*b*; Walderhaug & Bjørkum 1992; Prosser *et al.* 1993). This interpretation could be correct if it is assumed that calcite grew early (soon after deposition) at low temperature. An equivalent interpretation can be made for the Heather calcite $\delta^{18}O$ data reported here if the calcite is assumed to have developed at low temperature. Note that this interpretation appears to conflict with the model presented in Figure 21.

The calcite $\delta^{18}O$ values, therefore, can be used to confirm that calcite grew at relatively high temperature, in support of the evidence from high aqueous fluid inclusion homogenization temperatures and the presence of oil-filled primary inclusions within calcite. However, it is also possible that the some of the calcite $\delta^{18}O$ values may have resulted from growth at low temperature from mid to late Jurassic meteoric water percolating through the entire Brent sequence. Thus, from the $\delta^{18}O$ data it is possible that calcite cement in Heather has components of both eogenetic and mesogenetic growth (Figs 18 & 21).

Source of calcite cement and calcite localization within the Heather Field

Many earlier studies of diagenesis and reservoir quality invoked large-scale fluid flow and diffusion as being responsible for the presence of mineral cements in reservoir rocks; diagenesis was assumed to occur in a relatively open system (Glasmann *et al.* 1989*b*; Gluyas & Coleman 1992; Harrison & Thyne 1992; Hogg *et al.* 1993; McAulay *et al.* 1994; Brosse *et al.* 2003; Sanjuan *et al.* 2003). Recent developments in diagenesis and reservoir quality modelling have focused on the opposite assumption: that sandstone reservoirs largely represent closed geochemical systems and are thus isochemical (Lander & Walderhaug 1999; Walderhaug *et al.* 2000). It is likely that sandstone diagenetic systems will be relatively closed for low-solubility species such as Si, Al and Fe but may be relatively open for more soluble and mobile species such as Na, K and CO_2. Intermediate degrees of open v. closed behaviour may be anticipated for species with intermediate solubility, such as Ca and Mg (Worden *et al.* 2018*a*).

Many of the early studies of Brent diagenesis revealed a general lack of body fossils in the calcite-cemented horizons in the Brent Group. At the time, this was taken as firm evidence that the large volumes of calcite were not formed as a result of dissolution and re-precipitation of marine-derived $CaCO_3$. Large-scale fluid flow scenarios, including large-scale influx of meteoric water, were thus invoked to explain the calcite cement, including in the Heather Field (Glasmann *et al.* 1989*b*). Supporting evidence was sought in the interpretation of oxygen isotope data from calcite (e.g. Fig. 21). If low-temperature growth (i.e. <40°C) is assumed then the mean $\delta^{18}O$ value (e.g. −10‰ VPDB) was the result of calcite growth from water with a $\delta^{18}O$ value of about −6‰ VSMOW (Fig. 21); this coincides with values typical of meteoric water (Morad *et al.* 2003). In this scenario, the origin of the calcium in calcite was typically assigned to a range of internal sources including volcanic rock fragments and detrital calcium-bearing plagioclase (Morad & De Ros 1994) or the source of the calcium was not considered. Carbon isotope data were used to suggest that there was a range of sources for the carbonate (CO_2 or HCO_3) with the relatively negative range of $\delta^{13}C$ values indicative of a biogenic-derived

origin. Glasmann *et al.* (1989*a*) proposed that organic carbon in the calcite in the Heather Field was potentially sourced from the stratigraphically older (Lower Jurassic) shales of the Dunlin Group; they suggested that decarboxylation of organic matter in the Dunlin Shales may have released CO_2 that exhibited a strongly negative $\delta^{13}C$ signature.

A careful re-appraisal of the quantity of flowing water needed to produce the volume of calcite found in the Brent, using geochemical solubility models, concluded that each pore volume of calcite cement required a flux of 100 000–300 000 pore volumes of water and that this was simply not reasonable and should not be used as a basis upon which to develop a predictive model (Bjørkum & Walderhaug 1990*a*, b). Their work on strata-bound calcite in numerous sandstones in NW Europe led Bjørkum & Walderhaug (1990*a*) and Bjørkum & Walderhaug (1990*b*) to conclude that pore-filling calcite, such as that found in the Brent Group of the Heather Field, must have had internal sources and that bioclastic material is the most likely source, especially in the marine sandstones of the Brent Group. Note that either detrital micrite or marine carbonate cement, perhaps locally forming a hardground or distributed throughout the formation, may also have supplied some or most of the pore-filling calcite.

Middle Jurassic seawater had an $^{87}Sr/^{86}Sr$ ratio of 0.7073 and it is assumed that marine bioclastic fragments and detrital micrite would also have an $^{87}Sr/^{86}Sr$ ratio of 0.7073 (Veizer *et al.* 1999). $^{87}Sr/^{86}Sr$ values from calcite cement from the Brent, including those from the Heather Field, are typically greater than 0.7100 (Glasmann *et al.* 1989*a*; Prosser *et al.* 1993; Girard 1998). These elevated values were interpreted to show that the strontium in calcite (and by inference the calcium since these two elements have similar geochemical properties and behaviour) did not have a marine source. This interpretation is possibly incorrect since, as marine carbonate minerals dissolve and re-precipitate over time, they would be exposed to sources of radiogenic strontium (^{87}Sr) owing to the radioactive decay of ^{87}Rb, which is notably abundant in potassium minerals such as K-feldspar, muscovite and biotite (Krauskopf 1979), all of which are abundant in Brent sandstones. The elevated $^{87}Sr/^{86}Sr$ values in calcite cement may simply represent *in-situ* dissolution and re-precipitation of calcite in the presence of Brent Group formation waters, modified by ^{87}Rb breakdown in a relatively closed system.

So where did the large amount of calcite cement in the Brent Group of the Heather Field come from? Earlier conclusions (Glasmann *et al.* 1989*b*) about the calcite in Heather being the *result* of meteoric influx, with the carbonate solely deriving from organic sources, and the calcium not being the result of 'marine precipitation', are possibly incorrect. It is seemingly more likely that some or most of the calcite, notably localized to the marine part of the Brent Group, originated as bioclastic or micritic debris, or as marine cements, scattered throughout the formation or concentrated as hardgrounds. A dispersed mixture of bioclasts, micrite or marine cement composed of aragonite, high-Mg calcite and low-Mg calcite would have undergone progressive dissolution and re-precipitation during eodiagenesis, possibly continuing into mesodiagenesis, with the neoformed calcite growing as large poikilotopic crystals nucleating at a restricted number of sites. The newly forming calcite crystals would expand (poikilotopically) to encompass detrital quartz grains since it is energetically easier for an existing crystal to grow rather than for a totally new calcite crystal (calcite nucleus) to spontaneously nucleate (Berner 1980). These initial calcite crystals (e.g. Fig. 13a) seem to have grown into bigger nodules (Fig. 13b) and, in some case (Fig. 13c) develop into thick, strata-bound layers, all at the expense of the dispersed initial carbonate material (Bjørkum & Walderhaug 1990*a*, b). The lack of primary marine $\delta^{13}C$ values may simply reflect the sustained input of CO_2, or bicarbonate, from a range of sources during diagenesis, including bacterial oxidation, fermentation and decarboxylation, from stratigraphically and/or spatially related mudstones (intraformational shales, coals, etc., or from the Heather Formation top seal) (Macaulay *et al.* 1998). CO_2 was also generated in large volumes from the Kimmeridge Clay Formation source rock ahead of the main oil charge (Andresen *et al.* 1994), thus there have been numerous possible organic sources of CO_2, now locked up in calcite cement, that have operated throughout the basin history. It is also likely that the local input of biogenic CO_2 into pore fluids, needed to explain the range of calcite $\delta^{13}C$ values, might have caused localized and transient calcite dissolution with precipitation happening either when the CO_2 partial pressure decreased at that site or with diffusion of the dissolved calcite species to sites with lower CO_2 partial pressure (Worden & Barclay 2000). Note that the processes of dissolution and then re-precipitation would cause calcite to have its $\delta^{18}O$ values reset to represent the highest temperature of growth. Dissolution and then re-precipitation would also allow the calcite to become more ferroan and adopt radiogenic Sr isotope signals with increasing input of ^{87}Sr derived from the abundant ^{87}Rb that is present in potassic detrital minerals such as muscovite and K-feldspar (Table 2). Dissolution and then re-precipitation of calcite late in the burial history would have allowed the resulting calcite to develop high-temperature aqueous fluid inclusions and to trap oil inclusions in calcite. Variable degrees of calcite dissolution and re-precipitation can explain the calcite having many characteristics of early cement but

also presenting clear evidence of late diagenetic growth.

The lack of plagioclase in the Heather sandstones (Tables 1 & 2) may indicate one or more of the following: (1) sediment supply devoid of plagioclase; (2) plagioclase altered to clay minerals such as kaolinite during eodiagenesis; or (3) plagioclase alteration to kaolinite and possibly illite, during mesodiagenesis. Could plagioclase alteration have supplied the calcium in the abundant calcite cement in Heather? The answer is no since almost all sedimentary plagioclase is dominated by albite because the anorthite component is hugely unstable at the Earth's surface (Johnson & Basu 1993; Huang & Wang 2005); even if plagioclase is absent in Heather owing to eo- or meso-genetic reactions it would not have been Ca-rich and is highly unlikely to be capable of supplying sufficient calcium to generate the large volumes of calcite found. Moreover, it is not easy to understand why the calcite-cemented marine sediments would have been plagioclase-rich whereas the non-calcite cemented deltaic Ness sediments would have been plagioclase poor.

In summary, the calcite present in the Brent Group of the Heather Field was originally composed of one or more of marine micrite, bioclasts or marine cement that underwent dissolution, re-precipitation and rearrangement from dispersed micrite, bioclasts or early cement into highly concentrated calcite nodules that then merged to form strata-bound cemented horizons. This is supported by the marine facies of the host sedimentary rock, the high IGV (Table 1, Fig. 12) and the published modelling that discounts calcite cement owing to mass-flux into the sandstones (Bjørkum & Walderhaug 1990*a*, *b*). This process started soon after deposition and concluded after oil-filling commenced. Dissolution and then re-precipitation were probably induced by the primary deposition of unstable forms of carbonate (aragonite and high-Mg calcite) and the episodic influx of CO_2 from a range of biogenic sources (such as the Kimmeridge Clay Formation source rock), leading to transient under-saturation with calcite, over a long period of time.

Calcite distribution in the Heather Field

The interpreted seismic (Fig. 4) and wireline log (Figs 5 & 6) data show that there is more calcite on the flanks of the Heather Field than the crest, as well as revealing that there is much calcite in the marine lower Brent Formations. Note that if we assume that calcium in calcite was sourced from marine micrite, bioclasts or early marine cement then we cannot easily invoke localized and preferential growth of calcite from external sources of calcium in the flank regions; this line of reasoning will not be further developed. However, CO_2 is mobile in the subsurface and the calcite carbon isotopes reveal that there has been an influx of biogenic carbon, so influx of CO_2 into the Brent is highly likely.

The stratigraphic distribution is most simply explained by the Heather marine sediments containing micrite, bioclastic debris or early marine cements, common in shallow marine clastic sediment (Broom, Rannoch, Etive & Tarbert Formations). The delta-top deposits (Ness Formation) have little or no calcite because there was no primary micrite or bioclastics and no early marine cement.

The structural distribution of calcite is less easy to explain but there are three main possible ways to account for the crest–flank distribution:

(1) The structural distribution is an artefact of a primary depositional differences, e.g. the locations that are at today at the crest (Fig. 4) were originally deposited with less micrite or bioclastic material, or experienced less marine diagenesis, than the locations that are now at the flanks of the field. There are no reported sediment textural and sedimentary structure differences between the crest and flank sites of the marine part of the Brent reservoirs so that this explanation seems unlikely.

(2) The whole of the marine portions of the reservoir initially had abundant micrite, bioclasts or early marine $CaCO_3$ cement, but the crestal areas underwent preferential loss of $CaCO_3$ (e.g. dissolved and mobilized away from the crest to the flanks) early during the burial cycle (Burley 1993). This option was invoked previously for Brent diagenesis, with extensive meteoric water flushing used to explain kaolinite growth as well as calcite geochemical characteristics (Walderhaug & Bjørkum 1992). Several studies have invoked influxing meteoric water as a way of delivering calcite to the Broom (Glasmann *et al.* 1989*b*; Lundegard 1994) but the calcite solubility arguments reported previously (Bjørkum & Walderhaug 1990*a*) seem to discount this process. The feasibility of mass-loss of calcite from the present-day crestal regions, early in the burial history, could be tested by reaction-transport models of reconstructed middle and upper Jurassic geometries of the Brent fault blocks. Interestingly, Brosse *et al.* (2003) simulated meteoric water influx into Brent sediments and showed that there was an initial loss of calcite at the point of entry (percolation) of the meteoric water followed by no further significant loss of calcite as the meteoric water penetrated into the subsurface. If early diagenetic or detrital calcite has been locally lost from the present-day crest of the structure, micrite, bioclasts and

early calcite dissolution fabrics could be anticipated (especially at the boundary between the calcite cemented and non-cemented region) but evidence of this is lacking at the present time both from out work and previous Brent studies.

(3) The whole of the Broom Formation initially had abundant micrite, bioclasts or early marine $CaCO_3$ cement but the crestal areas underwent loss of $CaCO_3$ later during the burial cycle, e.g. owing to localized CO_2 influx causing mass dissolution of $CaCO_3$ and possible migration to the downdip and flank regions. A version of this option was invoked to explain the relative lack of calcite in Brent sediments at the crest of the Hild field (Lønøy *et al.* 1986). These authors suggested that a late influx of CO_2 caused extensive calcite dissolution and thus created secondary porosity as a result. The feasibility of mass loss of calcite from the present-day crestal regions, late in the burial history, could be tested by the reaction-transport model, based on the present-day geometries of the Brent fault blocks. The reported local link between calcite abundance with faults (Glasmann *et al.* 1989*b*) could conceivably be related to the influx of CO_2, along transiently open faults, and the resulting dissolution and either re-precipitation or re-distribution of calcite. If calcite has been locally lost from the present-day crest of the structure, diagenetically late calcite dissolution fabrics could be anticipated (again, especially at the boundary between the calcite cemented and non-cemented region), more work is required to assess this possibility.

Conclusions

(1) Calcite cement is found in large quantities in the marine units (Broom, Rannoch, Etive and Tarbert) of the Brent Group sandstones of the Heather oil field (UKCS); calcite occurs as cemented horizons and nodules in marine sediment, but is relatively rare in the non-marine, Ness Formation, units of the Brent Group.

(2) Evidence for the early growth of calcite (soon after deposition) includes high intergranular volume and the lack of compaction fabrics in pervasively calcite cemented samples.

(3) Evidence for the late growth of calcite (towards maximum burial and at much the same time as oil-filling) includes calcite growth after quartz cement, high aqueous fluid inclusion homogenization temperatures and the presence of oil-filled primary inclusions within calcite.

(4) At least some calcite growth occurred following quartz grain dissolution. This has led to some rather unusual clastic rocks now with 79% calcite with remaining micas picking out primary stratification and quartz grains more corroded and replaced than detrital feldspar grains. Dissolution and corrosion of quartz grains has been an important process in the calcite-cemented parts of the Brent Group.

(5) Calcite oxygen isotope data can be used to infer high temperature growth if calcite is assumed to be in equilibrium with present-day formation waters. However, if low-temperature growth is assumed then it can be inferred that calcite grew from late Jurassic meteoric water percolating into uplifted tilted fault blocks. Oxygen isotope data do not lead to an unequivocal interpretation.

(6) There is no direct evidence that a significant quantity of micrite or bioclasts was deposited in the Heather reservoir; however, others have reported belemnite and bivalve fragments in equivalent aged reservoir rocks in the North Sea Basin. The prevalence of calcite in the marine part of the Brent Group further supports a marine origin for calcite cement, possibly including micrite, bioclasts or early marine cement. The present distribution of calcite cement as cemented layers and nodules is probably the result of redistribution (self-organization) during burial owing to dissolution of primary or marine-diagenetic carbonate minerals (aragonite, high-Mg calcite), diffusion (or flow) and re-precipitation.

(7) Carbon isotope data from calcite strongly support the significant input of biogenic CO_2, e.g. from bacterial oxidation, fermentation or decarboxylation. This is not in conflict with a primary micrite, bioclast or early marine cement origin for calcite since an influx of CO_2 would have led to transient dissolution of marine carbonate followed by re-precipitation as CO_2 partial pressure subsided.

(8) The reservoir at the crest of the field has less calcite than at the flank of the field. This distribution could plausibly be explained by one or more of three different processes: differing amounts of calcite present at the time of deposition that coincidentally now relate to crest v. flank locations; localized removal of primary calcite from the crest soon after deposition, e.g. during eogenetic meteoric flux into present-day crestal sites; localized removal of primary calcite from the crest late in the history, e.g. during mesogenetic CO_2 flux into crestal sites. Further studies are needed to narrow down which of these options are more likely.

Acknowledgements This study was a collaborative project between the University of Liverpool and EnQuest, Aberdeen. EnQuest are thanked for providing the seismic section, the wireline data and the core analysis. We also wish to thank Steve Crowley and James Utley for carrying out stable isotope and SEM-EDS analyses, respectively. Finally, FEI are thanked for providing the SEM-EDS system. Editor Patrick Dowey and two anonymous reviewers are thanked for constructive and positive comments on an earlier version of this manuscript.

References

Andresen, B., Throndsen, T., Barth, T. & Bolstad, J. 1994. Thermal generation of carbon dioxide and organic acids from different source rocks. *Organic Geochemistry*, **21**, 1229–1242, https://doi.org/10.1016/0146-6380(94)90166-X

Armitage, P.J., Worden, R.H., Faulkner, D.R., Aplin, A.C., Butcher, A.R. & Iliffe, J. 2010. Diagenetic and sedimentary controls on porosity in Lower Carboniferous fine-grained lithologies, Krechba field, Algeria: a petrological study of a caprock to a carbon capture site. *Marine and Petroleum Geology*, **27**, 1395–1410, https://doi.org/10.1016/j.marpetgeo.2010.03.018

Ashcroft, W.A. & Ridgway, M.S. 1996. Early discordant diagenesis in the Brent Group, Murchison Field, UK North Sea, detected in high values of seismic-derived acoustic impedance. *Petroleum Geoscience*, **2**, 75–81, https://doi.org/10.1144/petgeo.2.1.75

Beard, D.C. & Weyl, P.K. 1973. Influence of texture on porosity and permeability of unconsolidated sand. *American Association of Petroleum Geologists Bulletin*, **57**, 349–369.

Benbaccar, M., Fritz, B., Sommer, F., Bazin, B. & Brosse, E. 1995. Geochemical modelling of mineral diagenesis in the Brent sandstone reservoirs, Alwyn South and Alwyn North areas, East Shetland Basin, North Sea. *Water–Rock Interaction*, 437–440.

Berner, R.A. 1980. *Early Diagenesis, a Theoretical Approach*. Princeton University Press, Princeton, NJ.

Bjørkum, P.A. 1996. How important is pressure in causing dissolution of quartz in sandstones? *Journal of Sedimentary Research*, **66**, 147–154, https://doi.org/10.1306/D42682DE-2B26-11D7-8648000102C1865D

Bjørkum, P.A. & Walderhaug, O. 1990*a*. Geometrical arrangement of calcite cementation within shallow marine sandstones. *Earth-Science Reviews*, **29**, 145–161, https://doi.org/10.1016/0012-8252(0)90033-R

Bjørkum, P.A. & Walderhaug, O. 1990*b*. Lateral extent of calcite cemented zones in shallow marine sandstones. *In*: Buller, A.T., Berg, E., Hjelmeland, O., Kleppe, J., Torsaeter, O. & Aasen, J.O. (eds) *2nd Interntational Conference on North Sea Oil and Gas Reservoirs-II (the University of Trondheim)*. Graham and Trotman, London, 331–336.

Bjørlykke, K., Nedkvitne, T., Ramm, M. & Saigal, G. 1992. Diagenetic processes in the Brent Group (Middle Jurassic) reservoirs of the North Sea: an overview. *In*: Morton, A.C., Haszeldine, R.S., Giles, M.R. & Brown, S. (eds) *Geology of the Brent Group*. Geological Society, London, Special Publications, **61**, 263–287, https://doi.org/10.1144/GSL.SP.1992.061.01.15

Brosse, E., Margueron, T. *et al*. 2003. The formation and stability of kaolinite in Brent sandstone reservoirs: a modelling approach. *In*: Worden, R.H. & Morad, S. (eds) *Clay Mineral Cements in Sandstones*. Special Publications of the International Association of Sedimentologists, **34**. Blackwells, Oxford, 383–410.

Bryant, I.D., Kantorowicz, J.D. & Love, C.F. 1988. The origin and recognition of laterally continuous carbonate cemented horizons in the Upper Lias sands of Southern England. *Marine and Petroleum Geology*, **5**, 108–133, https://doi.org/10.1016/0264-8172(88)90018-9

Burley, S.D. 1993. Models of burial diagenesis for deep exploration plays in Jurassic fault traps of the Central and Northern North Sea. *In*: Parker, J.R. (ed.) *Petroleum Geology of Northwest Europe: Proceedings of the 4th Conference*. Geological Society, London, 1353–1375, https://doi.org/10.1144/0041353

Clauer, N. & Liewig, N. 2013. Episodic and simultaneous illitisation in oil-bearing Brent Group and Fulmar Formation sandstone from the northern and southern North Sea based on illite K–Ar dating. *American Association of Petroleum Geologists Bulletin*, **97**, 2149–2171, https://doi.org/10.1306/04021312122

Deegan, C.E. & Scull, B.J. 1977. *A Standard Lithostratigraphic Nomenclature for the Central and Northern North Sea*. Report of the Institute of Geological Sciences.

Dutton, S.P. 1997. Timing of compaction and quartz cementation from integrated petrographic and burial-history analyses, Lower Cretaceous Fall River Formation, Wyoming and South Dakota. *Journal of Sedimentary Research*, **67**, 186–196, https://doi.org/10.1306/D426852C-2B26-11D7-8648000102C1865D

Ehrenberg, S.N. 1995. Measuring sandstone compaction from modal analysis of thin sections – how to do it and what the results mean. *Journal of Sedimentary Research Section a – Sedimentary Petrology and Processes*, **65**, 369–379, https://doi.org/10.1306/D42680C7-2B26-11D7-8648000102C1865D

Ehrenberg, S.N. 1997. Influence of depositional sand quality and diagenesis on porosity and permeability: examples from Brent Group Reservoirs, northern North Sea (vol 67, pg 202, 1997). *Journal of Sedimentary Research*, **67**, 618–618.

Ehrenberg, S.N. & Jakobsen, K.G. 2001. Plagioclase dissolution related to biodegradation of oil in Brent Group sandstones (Middle Jurassic) of Gullfaks Field, northern North Sea. *Sedimentology*, **48**, 703–721, https://doi.org/10.1046/j.1365-3091.2001.00387.x

EnQuest, 2018. Heather redevelopment. http://www.enquest.com/our-business/developments/heather-redevelopment.aspx

Friedman, I. & O'Neil, J.R. 1977. Compilation of stable isotope fractionation factors of geochemical interest. *US Geological Survey Professional papers*, Data of Geochemistry.

Giles, M.R., Stevenson, S., Martin, S.V., Cannon, S.J.C., Hamilton, P.J., Marshall, J.D. & Samways, G.M. 1992. The reservoir properties and diagenesis of the Brent Group: a regional perspective. *In*: Morton, A.C., Haszeldine, R.S., Giles, M.R. & Brown, S. (eds) *Geology of the Brent Group*. Geological Society, London, Special Publications, **61**, 289–327, https://doi.org/10.1144/GSL.SP.1992.061.01.16

Girard, J.P. 1998. Carbonate cementation in the Middle Jurassic Oseburg reservoir sandstone, Oseburg field, Norway: a case of deep burial-high temperature poikilotopic calcite. *In*: Morad, S. (ed.) *Carbonate Cementation in Sandstones*. Special Publications of the International Association of Sedimentologists, **26**. Blackwells, Oxford, 285–308.

Girard, J.P., Munz, I.A., Johansen, H., Hill, S. & Canham, A. 2001. Conditions and timing of quartz cementation in Brent reservoirs, Hild Field, North Sea: constraints from fluid inclusions and SIMS oxygen isotope microanalysis. *Chemical Geology*, **176**, 73–92, https://doi.org/10.1016/S0009-2541(00)00350-8

Girard, J.P., Munz, I.A., Johansen, H., Lacharpagne, J.C. & Sommer, F. 2002. Diagenesis of the Hild Brent sandstones, northern North Sea: isotopic evidence for the prevailing influence of deep basinal water. *Journal of Sedimentary Research*, **72**, 746–759, https://doi.org/10.1306/040102720746

Glasmann, J.R. 1992. The fate of feldspar in Brent Group reservoirs, North Sea: a regional synthesis of diagenesis in shallow, intermediate, and deep burial environments. *In*: Morton, A.C., Haszeldine, R.S., Giles, M.R. & Borown, S. (eds) *Geology of the Brent Group*. Geological Society, London, Special Publications, **61**, 329–350, https://doi.org/10.1144/GSL.SP.1992.061.01.01

Glasmann, J.R., Clark, R.A., Larter, S., Briedis, N.A. & Lundegard, P.D. 1989*a*. Diagenesis and hydrocarbon accumulation, Brent sandstone (Juassic), Bergen High Area, North Sea. *American Association of Petroleum Geologists Bulletin*, **73**, 1341–1360.

Glasmann, J.R., Lundegard, P.D., Clark, R.A., Penny, B.K. & Collins, I.D. 1989*b*. Geochemical evidence for the history of diagenesis and fluid migration – Brent Sandstone, Heather Field, North Sea. *Clay Minerals*, **24**, 255–284, https://doi.org/10.1180/claymin.1989.024.2.10

Gluyas, J. & Coleman, M. 1992. Material flux and porosity changes during sediment diagenesis. *Nature*, **356**, 52–54, https://doi.org/10.1038/356052a0

Goldstein, R.H. & Reynolds, T.J. 1994. *Systematics of Fluid Inclusions in Diagenetic Minerals*. SEPM Short course, Society for Sedimentary Geology, Tulsa, OK.

Guilhaumou, N., Cordon, S., Durand, C. & Sommer, F. 1998. P-T conditions of sandstones silicification from the Brent Group (Dunbar, North Sea). *European Journal of Mineralogy*, **10**, 355–366, https://doi.org/10.1127/ejm/10/2/0355

Hampson, G.J., Sixsmith, P.J. & Johnson, H.D. 2004. A sedimentological approach to refining reservoir architecture in a mature hydrocarbon province: the Brent Province, UK North Sea. *Marine and Petroleum Geology*, **21**, 457–484, https://doi.org/10.1016/S0264-8172(03)00094-1

Harris, N.B. 1989. Diagenetic quartzarenite and destruction of secondary porosity – an example from the Middle Jurassic Brent Sandstone of Northwest Europe. *Geology*, **17**, 361–364, https://doi.org/10.1130/0091-7613(1989)017<0361:DQADOS>2.3.CO;2

Harris, N.B. 1992. Burial diagenesis of Brent sandstones: a study of Statfjord, Hutton and Lyell fields. *In*: Morton, A.C., Haszeldine, R.S., Giles, M.R. & Brown, S. (eds) *Geology of the Brent Group*. Geological Society, London, Special Publications, **61**, 351–375, https://doi.org/10.1144/GSL.SP.1992.061.01.18

Harrison, W.J. & Thyne, G.D. 1992. Predictions of diagenetic reactions in the presence of organic acids. *Geochimica et Cosmochimica Acta*, **56**, 565–586, https://doi.org/10.1016/0016-7037(92)90082-T

Hassouta, L., Buatier, M.D., Potdevin, J.L. & Liewig, N. 1999. Clay diagenesis in the sandstone reservoir of the Ellon Field (Alwyn, North Sea). *Clays and Clay Minerals*, **47**, 269–285, https://doi.org/10.1346/CCMN.1999.0470303

Haszeldine, R.S., Brint, J.F., Fallick, A., Hamilton, P.J. & Brown, S. 1992. Open and restricted hydrologies in Brent Group diagenesis: North Sea. *In*: Morton, A.C., Haszeldine, R.S., Giles, M.R. & Brown, S. (eds) *Geology of the Brent Group*. Geological Society, London, Special Publications, **61**, 401–419, https://doi.org/10.1144/GSL.SP.1992.061.01.20

Helle, K. & Helland-Hansen, W. 2009. Genesis of an over-thickened shoreface sandstone tongue: the Rannoch and Etive formations of the Middle Jurassic Brent delta, North Sea. *Basin Research*, **21**, 620–643, https://doi.org/10.1111/j.1365-2117.2009.00395.x

Hogg, A.J.C., Sellier, E. & Jourdan, A. 1992. Cathodoluminescence of quartz cements in Brent Group sandstones, Alwyn South, UK North Sea. *In*: Morton, A.C., Haszeldine, R.S., Giles, M.R. & Brown, S. (eds) *Geology of the Brent Group*. Geological Society, London, Special Publications, **61**, 421–440, https://doi.org/10.1144/GSL.SP.1992.061.01.21

Hogg, A.J.C., Hamilton, P.J. & Macintyre, R.M. 1993. Mapping diagenetic fluid-flow within a reservoir – K–Ar dating in the Alwyn area (UK North Sea). *Marine and Petroleum Geology*, **10**, 279–294, https://doi.org/10.1016/0264-8172(93)90110-E

Hogg, A.J.C., Pearson, M.J., Fallick, A.E. & Hamilton, P.J. 1995. An integrated thermal and isotopic study of the diagenesis of the Brent Group, Alwyn South, UK North Sea. *Applied Geochemistry*, **10**, 531–5–&, https://doi.org/10.1016/0883-2927(95)00024-0

Houseknecht, D.W. 1987. Assessing the relative importance of compaction processes and cementation to reduction of porosity in sandstones. *American Association of Petroleum Geologists Bulletin*, **71**, 633–642.

Huang, P.M. & Wang, M.K. 2005. Minerals, primary. *In*: Hillel, D. (ed.) *Encyclopedia of Soils in the Environment*. Elsevier, Amsterdam, 500–510.

Johnson, M.J. & Basu, A. 1993. *Processes Controlling the Composition of Clastic Sediments*. GSA Special Papers, **284**, Geological Society of America, Boulder, Colorado.

Kay, S. 2003. The heather field, Block 2/5, UK North Sea. *In*: Gluyas, J.G. & Hichens, H.M. (eds) *United Kingdom Oil and Gas Fields, Commemerative Millenium Volume*. Geological Society, London, Memoirs, **20**, 291–304.

Kay, S. & Cuddy, S. 2002. Innovative use of petrophysics in field rehabilitation, with examples from the Heather Field. *Petroleum Geoscience*, **8**, 317–325, https://doi.org/10.1144/petgeo.8.4.317

Krauskopf, K.B. 1979. *Introduction to Geochemisty*. McGraw-Hill, Tokyo.

Lander, R.H. & Walderhaug, O. 1999. Predicting porosity through simulating sandstone compaction and quartz

cementation. *American Association of Petroleum Geologists Bulletin*, **83**, 433–449.

Lønøy, A., Akselsen, J. & Ronning, K. 1986. Diagenesis of a deeply buried sandstone reservoir: Hild Field, Northern North Sea. *Clay Minerals*, **21**, 497–511, https://doi.org/10.1180/claymin.1986.021.4.06

Loseth, T.M. & Ryseth, A. 2003. A depositional and sequence stratigraphic model for the Rannoch and Etive formations, Oseberg Field, northern North Sea. *Norwegian Journal of Geology*, **83**, 87–106.

Lundegard, P.D. 1994. Mixing zone origin of C-13-depleted calcite cement – Oseberg Formation Sandstones (Middle Jurassic), Veslefrikk Field, Norway. *Geochimica et Cosmochimica Acta*, **58**, 2661–2675, https://doi.org/10.1016/0016-7037(94)90136-8

Macaulay, C.I., Fallick, A., McLaughlin, O.M., Haszeldine, R.S. & Pearson, M.J. 1998. The significance of $\delta^{13}C$ of carbonate cement in reservoir sandstones; a regional perspective from the Jurassic of the Northern North Sea. *In*: Morad, S. (ed.) *Carbonate Cementation in Sandstones*. Special Publications of the International Association of Sedimentologists, **26**, Blackwells, Oxford, 395–408.

McAulay, G.E., Burley, S.D., Fallick, A.E. & Kusznir, N.J. 1994. Palaeohydrodynamic fluid flow regimes during diagenesis of the Brent Group in the Hutton–NW Hutton reservoirs – constraints from oxygen isotope studies of authigenic kaolinite and reverse flexural modelling. *Clay Minerals*, **29**, 609–626, https://doi.org/10.1180/claymin.1994.029.4.16

Morad, S. & De Ros, L.F. 1994. Geochemistry and diagenesis of stratabound calcite cement layers within the Rannoch Formation of the Brent Group, Murchison Field, North Viking Graben (Northern North Sea) – Comment. *Sedimentary Geology*, **93**, 135–141, https://doi.org/10.1016/0037-0738(94)90032-9

Morad, S., Worden, R.H. & Ketzer, J.M. 2003. Oxygen and hydrogen isotopic composition of diagenetic clay minerals in sandstones: a review of the data and controls. *In*: Worden, R.H. & Morad, S. (eds) *Clay Mineral Cements in Sandstones*. Special Publications of the International Association of Sedimentologists, **34**, Blackwells, Oxford, 63–91.

Morris, J.E., Hampson, G.J. & Johnson, H.D. 2006. A sequence stratigraphic model for an intensely bioturbated shallow-marine sandstone: the Bridport Sand Formation, Wessex Basin, UK. *Sedimentology*, **53**, 1229–1263, https://doi.org/10.1111/j.1365-3091.2006.00811.x

Munz, I.A., Wangen, M., Girard, J.P., Lacharpagne, J.C. & Johansen, H. 2004. Pressure–temperature–time–composition (*P–T–t–X*) constraints of multiple petroleum charges in the Hild field, Norwegian North Sea. *Marine and Petroleum Geology*, **21**, 1043–1060, https://doi.org/10.1016/j.marpetgeo.2004.05.006

Nedkvitne, T. & Bjørlykke, K. 1992. Secondary porosity in the Brent Group (Middle Jurassic), Huldra Field, North Sea: implication for predicting lateral continuity of sandstones? *Journal of Sedimentary Petrology*, **62**, 23–34, https://doi.org/10.1306/D426787A-2B26-11D7-8648000102C1865D

Osborne, M., Haszeldine, R.S. & Fallick, A.E. 1994. Variations in kaolinite morphology with growth temperature in isotopically mixed pore-fluids, Brent Group, UK North Sea. *Clay Minerals*, **29**, 591–608, https://doi.org/10.1180/claymin.1994.029.4.15

Penny, B.K. 1991. The Heather Field, Block 2/5, UK North Sea. *In*: Abbotts, I.L. (ed.) *United Kingdom Oil and Gas Fields 25 Years Commemorative Volume*. Geological Society, London, Memoirs, **14**, 127–134.

Pirrie, D., Butcher, A.R., Power, M.R., Gottlieb, P. & Miller, G.L. 2004. Rapid quantitative mineral and phase analysis using automated scanning electron microscopy (QemSCAN): potential applications in forensic geoscience. *In*: Pye, K. & Croft, D.J. (eds) *Forensic Geoscience: Principles, Techniques and Applications*. Geological Society, Bath, **232**, 123–136.

Potdevin, J.L. & Hassouta, L. 1997. Mass balance of illitization and quartz overgrowth in the sandstone reservoir of the Ellon field (Alwyn, North Sea). *Bulletin De La Societe Geologique De France*, **168**, 219–229.

Prosser, D.J., Daws, J.A., Fallick, A.E. & Williams, B.P.J. 1993. Geochemistry and diagenesis of stratabound calcite cement layers within the Rannoch Formation of the Brent Group, Murchison Field, North Viking Graben (Northern North Sea). *Sedimentary Geology*, **87**, 139–164, https://doi.org/10.1016/0037-0738(93)90002-M

Prosser, D.J., Fallick, A.E., Daws, J.A. & Williams, B.P.J. 1994. Geochemistry and diagenesis of stratabound calcite cement layers within the Rannoch Formation of the Brent Group, Murchison Field, North Viking Graben (Northern North Sea) – reply. *Sedimentary Geology*, **93**, 143–147, https://doi.org/10.1016/0037-0738(94)90033-7

Richards, P.C. 1992. An introduction to the Brent Group: a literature review. *In*: Morton, A.C., Haszeldine, R.S., Giles, M.R. & Brown, S. (eds) *Geology of the Brent Group*. Geological Society, London, Special Publications, **61**, 15–26, https://doi.org/10.1144/GSL.SP.1992.061.01.03

Ronning, K. & Steel, R. 1987. Depositional sequences within a 'transgressive' reservoir sandstone unit: the middle Jurassic Tarbert formation, Hild area, northern North Sea. *In*: Kleppe, J., Berg, E.W., Buller, A.T., Hjelmeland, O. & Torsaeter, O. (eds) *North Sea Oil and Gas Reservoirs*. Graham & Trotman, London, 169–176.

Ryseth, A. 2000. Differential subsidence in the Ness Formation (Bajocian), Oseberg area, northern North Sea: facies variation, accommodation space development and sequence stratigraphy in a deltaic distributary system. *Norsk Geologisk Tidsskrift*, **80**, 9–25, https://doi.org/10.1080/002919600750042645

Saigal, G.C. & Bjørlykke, K. 1987. Carbonate cements in clastic reservoir rocks from offshore Norway – relationships between isotopic composition, textural development and burial depth. In: Marshall, J. D. (ed.) *Diagenesis of Sedimentary Sequences*. Geological Society, London, Special Publications, **36**, 313–324, https://doi.org/10.1144/GSL.SP.1987.036.01.22

Sanjuan, B., Girard, J.P., Lanini, S., Bourguinon, A. & Brosse, E. 2003. Geochemical modelling of diagenetic illite and quartz cement formation in Brent sandstone reservoirs: example of the Hild Field, Norwegian North Sea. *In*: Worden, R.H. & Morad, S. (eds) *Clay Mineral Cements in Sandstones*. Special Publications of the International Association of Sedimentologists, **34**, Blackwells, Oxford, 425–452.

Scotchman, I.C., Johnes, L.H. & Miller, R.S. 1989. Clay diagenesis and oil migration in Brent Group sandstones of NW Hutton Field, UK North-Sea. *Clay Minerals*, **24**, 339–374, https://doi.org/10.1180/claymin.1989.024.2.13

Spotl, C. & Wright, V.P. 1992. Groundwater dolocretes from the Upper Triassic of the Paris basins, France – a case study of an arid continental diagenetic facies. *Sedimentology*, **39**, 1119–1136, https://doi.org/10.1111/j.1365-3091.1992.tb02000.x

Spotl, C., Matter, A. & Brevart, O. 1993. Diagenesis and pore water evolution in the Keuper reservoir, Paris Basin (France). *Journal of Sedimentary Petrology*, **63**, 909–928, https://doi.org/10.1306/D4267C44-2B26-11D7-8648000102C1865D

Stephenson, L.P., Plumley, W.J. & Palciauskas, V.V. 1992. A model for sandstone compaction by grain interpenetration. *Journal of Sedimentary Petrology*, **62**, 11–22, https://doi.org/10.1306/D4267875-2B26-11D7-8648000102C1865D

Veizer, J., Ala, D. *et al.* 1999. $^{87}Sr/^{86}Sr$, $\delta^{13}C$ and $\delta^{18}O$ evolution of Phanerozoic seawater. *Chemical geology*, **161**, 59–88, https://doi.org/10.1016/S0009-2541(99)00081-9

Vieira, M.M., De Ros, L.F. & Bezerra, F.H.R. 2007. Lithofaciology and palaeoenvironmental analysis of Holocene beachrocks in northeastern Brazil. *Journal of Coastal Research*, **23**, 1535–1548, https://doi.org/10.2112/05-0562.1

Walderhaug, O. 2000. Modeling quartz cementation and porosity in Middle Jurassic Brent Group sandstones of the Kvitebjorn field, Northern North Sea. *American Association of Petroleum Geologists Bulletin*, **84**, 1325–1339, https://doi.org/10.1306/A9673E96-1738-11D7-8645000102C1865D

Walderhaug, O. & Bjørkum, P.A. 1992. Effect of meteoric water-flow on calcite cementation in the Middle Jurassic Oseberg Formation, well 30/3-2, Veslefrikk Field, Norwegian North Sea. *Marine and Petroleum Geology*, **9**, 308–318, https://doi.org/10.1016/0264-8172(92)90079-T

Walderhaug, O., Lander, R.H., Bjørkum, P.A., Oelkers, E.H., Bjørlykke, K. & Nadeau, P.H. 2000. Modelling quartz cementation and porosity in reservoir sandstones: examples from the Norwegain continental shelf. *In*: Worden, R.H. & Morad, S. (eds) *Quartz Cementation in Sandstones*. Special Publication of the International Association of Sedimentologists, **29**, Blackwells, Oxford, 39–50.

Warren, E.A. & Smalley, P.C. 1994. North Sea formation water atlas. *Geological Society of London Memoir*, **15**, 208.

Went, D.J., Hamilton, R.V., Platt, N.H. & Underhill, J.R. 2013. Role of forced regression in controlling Brent Group reservoir architecture and prospectivity in the northern North Sea. *Petroleum Geoscience*, **19**, 307–328, https://doi.org/10.1144/petgeo2013-028

Wilkinson, M., Haszeldine, R.S., Ellam, R.M. & Fallick, A. 2004. Hydrocarbon filling history from diagenetic evidence: Brent Group, UK North Sea. *Marine and Petroleum Geology*, **21**, 443–455, https://doi.org/10.1016/S0264-8172(03)00092-8

Worden, R.H. 1998. Dolomite cement distribution in a sandstone from core and wireline data: the Triassic fluvial Chaunoy Formation, Paris Basin. *In*: Harvey, P.K. & Lovell, M.A. (eds) *Core-Log Integration*, Geological Society, London, **136**, 197–211.

Worden, R.H. & Barclay, S.A. 2000. Internally-sourced quartz cement due to externally-derived CO_2 in subarkosic sandstones, North Sea. *Journal of Geochemical Exploration*, **69**, 645–649, https://doi.org/10.1016/S0375-6742(00)00104-7

Worden, R.H. & Matray, J.M. 1998. Carbonate cements in the Triassic Chaunoy Formation of the Paris Basin: distribution and effect on fluid flow properties. *In*: Morad, S. (ed.) *Carbonate Cementation in Sandstones*. International Association of Sedimentologists Special Publications, **26**. Blackwells, Oxford, 163–178.

Worden, R.H., Warren, E.A., Smalley, P.C., Primmer, T.J. & Oxtoby, N.H. 1995. Evidence for resetting of fluid inclusions from quartz cements in oil fields – discussion. *Marine and Petroleum Geology*, **12**, 566–570, https://doi.org/10.1016/0264-8172(95)90014-4

Worden, R.H., Coleman, M.L. & Matray, J.M. 1999. Basin scale evolution of formation waters: a diagenetic and formation water study of the Triassic Chaunoy Formation, Paris Basin. *Geochimica et Cosmochimica Acta*, **63**, 2513–2528, https://doi.org/10.1016/S0016-7037(99)00121-0

Worden, R.H., Benshatwan, M.S., Potts, G.J. & Elgarmadi, S.M. 2016. Basin-scale fluid movement patterns revealed by veins. *Wessex Basin, UK: Geofluids*, **16**, 149–174, https://doi.org/10.1111/gfl.12141

Worden, R.H., Armitage, P.J. *et al.* 2018*a*. Petroleum reservoir quality prediction: overview and contrasting approaches from sandstone and carbonate communities. *In*: Armitage, P.J., Butcher, A. *et al.* (eds) *Reservoir Quality of Clastic and Carbonate Rocks: Analysis, Modelling and Prediction*. Geological Society, London, Special Publications, **435**, 1–31, https://doi.org/10.1144/SP435.21

Worden, R.H., Utley, J.E.P., Butcher, A.R., Griffiths, J., Wooldridge, L.J. & Lawan, A.Y. 2018*b*. Improved imaging and analysis of chlorite in reservoirs and modern day analogues: new insights for reservoir quality and provenance. *In*: Dowey, P.J., Osborne, M.J. & Volk, H. (eds) *Application of Analytical Techniques to Petroleum Systems*. Geological Society, London, Special Publications, **484**, https://doi.org/10.1144/SP484.10

Ziegler, K., Coleman, M.L. & Howarth, R.J. 2001. Palaeohydrodynamics of fluids in the Brent Group (Oseberg Field, Norwegian North Sea) from chemical and isotopic compositions of formation waters. *Applied Geochemistry*, **16**, 609–632, https://doi.org/10.1016/S0883-2927(00)00057-3